Mineralogy and Geochemistry of the Paleocene-Eocene Palana Formation in Western Rajasthan, India: Insights for Sedimentary Paleoenvironmental Conations and Volcanic Activity

Mohammed Hail Hakimi *, Alok Kumar, Abdullah Alqubalee, Alok Singh, Mohammed Almobarky, Afikah Rahim, Mohammad Alqudah, Aref Lashin, Khairul Azlan Mustapha, Waqas Naseem

Posted Date: 24 November 2023

doi: 10.20944/preprints202311.1550.v1

Keywords: organic-rich shale; bioproductivity; anoxia conditions; organic accumulation; Rajasthan; western India

Article

Mineralogy and Geochemistry of the Paleocene-Eocene Palana Formation in Western Rajasthan, India: Insights for Sedimentary Paleoenvironmental Conations and Volcanic Activity

Mohammed Hail Hakimi [1,*], Alok Kumar [2], Abdullah M. Alqubalee [3], Alok K. Singh [4], Mohammed Almobarky [5], Afikah Rahim [6], Mohammad Alqudah [7], Aref Lashin [5], Khairul Azlan Mustapha [2] and Waqas Naseem [8]

1 Department of Petroleum Engineering, Kazan Federal University, Kazan 420008, Russia
2 Department of Geology, University of Malaya, Kuala Lumpur, Malaysia
3 Center for Integrative Petroleum Research, 5College of Petroleum Engineering and ?Geosciences, King Fahd University of Petroleum and Minerals, Dhahran, 31261, Saudi Arabia
4 Rajiv Gandhi Institute of Petroleum Technology, Jais, India
5 College of Engineering, Petroleum and Natural Gas Engineering Department, King Saud University, Riyadh 11421-Saudi Arabia
6 Department of Geotecnics & Transportation, Faculty of Civil Engineering, Universiti Teknologi Malaysia, 81310 Johor Bahru, Malaysia
7 Department of Earth and Environmental Sciences, Yarmouk University, Shafeeq Irsheidat Street, 21163 Irbid, Jordan
8 Department of Geology, University of Poonch Rawalakot, Azad Jammu& Kashmir Rawalakot 12350, Pakistan
* Correspondence: ibnalhakimi@taiz.edu.ye

Abstract: Organic-rich shale deposits of the Paleocene-Eocene Palana Formation in western Rajasthan, India were systematically analyzed based on the elemental composition and organic geochemistry combined with microscopic examinations to evaluate the sedimentary paleoenvironmental conations and volcanic activity and their impact on the high organic carbon accumulation. The Palana shales are categorized by high OM and sulfur contents with total values up to 36.23 wt. % and 2.24 wt. %, respectively, suggesting marine setting and anoxic environmental conditions during the Paleocene-Eocene period. The richness of phytoplankton algae (i.e., telalginite and lamalginite) together with redox-sensitive trace elements further suggests anoxic environmental conditions. The significant low oxygen conditions may contributes to enhance preservation of organic matter during deposition. The mineralogical and inorganic geochemical indicators demonstrate that the Palana organic-rich shale facies was accumulated in warm and humid climate and low salinity stratification conditions of the water columns, thereby contributing to high bioproductivity of the phytoplankton algae blooms within the photic zone. The presence of the high concentrations of Fe-rich silica minerals such as olivine in most of the Palana organic-rich shales facility volcanic origin and supports hydrothermal activities during the Paleocene-Eocene period. These volcanic activities in this case are considered influx of large masses of nutrients into the photic zone due to the ash accumulation. Therefore, high bio-productivity associated with effective OM preservation contributed to the organic carbon accumulation in the Palana Formation during the Paleocene-Eocene.

Keywords: organic-rich shale; bioproductivity; anoxia conditions; organic accumulation; Rajasthan; western India

 doi:10.20944/preprints202311.1550.v1

1. Introduction

Black shale sedimentary rocks, commonly referred to as organic-rich mudstone and oil shale, which are of great interest globally owing to their potential for source and reservoir of the hydrocarbon accumulation (Jarvie et al., 2007; Sohail et al., 2022). However, both marine and continental black shales have received increased attention for conventional and unconventional petroleum resources because of the increasing energy demands (Jarvie et al., 2007; Mukherjee and Misra 2018; Sohail et al., 2022). However, most of the back shale sediments contain appreciable amounts of organic matter of more than 1 wt.% and were mainly accumulated under anoxic bottom water conditions in the marine and continental sedimentary basins (e.g., Hakimi et al., 2011 and 2013; Makeen et al., 2015 and 2019; Hatem et al., 2016; Ahmed et al., 2022).

However, the diagenesis and accumulation of the organic matter (OM) in these organic-rich shale sediments seriously limit by several factors such as biological productivity, continental weathering, sedimentation rates, clay mineralogy, water column oxygenation levels, sea-level change, and sedimentary environment of these shales (Li et al., 2008; Zonneveld et al., 2010; Bechtel et al., 2012; Shu et al., 2013 among many others). The productivity of organism together with preservation and degradation of the organic matter are the most important factors responsible for organic-matter enrichment (Calvert and Pedersen, 1992; Bordenave, 1993; Schwarzkopf, 1993; Carroll and Bohacs, 1999). The bioproductivity is one of the major factors controlling the organic matter input, whereas the absence or the depletion of dissolved oxygen in bottom waters foster the preferential accumulation and preservation of organic matter (OM) in sediments (Katz, 2005; Hakimi et al., 2016; Jia et al., 2013; Mohialdeen et al., 2013). In this regard, multi-integrated analytical methods are vital to the study of the organic-rich shale systems, where organic and inorganic geochemistry combined with microscopic examination can be used to assess the origin of organic matter input and their characteristics resulting from sedimentary factors influencing the organic matter (OM) accumulation (Hakimi et al., 2016; Jia et al., 2013; Mohialdeen et al., 2013).

The key focus of the present study is the Rajasthan stat, which is one of the largest hydrocarbon-containing sedimentary basins in western India (Directorate General of Hydrocarbons, India). Rajasthan, which is a part of the Indian Shield, contains four basins; the Barmer, Bikaner-Nagaur, Jaisalmer, and Sanchore Basins (Figure 1), which were developed by intracratonic sedimentation and are mostly located in the western part of Rajasthan. These basins feature a huge lignite reserve containing thick organic-rich black shale partings, which are mainly found in the Paleogene–Eocene sequences (Singh et al. 2020; Kumar et al. 2020, 2022). In this case, the current research focuses on the organic matter-bearing black shale sediments, particularly those of the Paleogene–Eocene Palana Formation. The black shale deposits of the Palana Formation mainly occur in the Gurha areas of the Bikaner-Nagaur Basin (Singh et al. 2020). The Palana's black shales are enriched in sapropelic OM, with an unimportant admixture of humic and/or zoogenic substances locally (Singh et al. 2020).

The Palana Formation has attracted the attention of academia and exploration companies due to the presence of superior source rocks and hydrocarbon generation potential. However, the lignite deposits in the Palana Formation have been extensively investigated by many researchers to characterize their organic matter and depositional setting and evaluate their hydrocarbon-generation potential (Singh et al. 2016; Singh and Kumar 2017; Singh and Kumar 2018; Kumar et al. 2020; Mathews et al. 2020; Kumar 2022; Singh et al. 2022) using the advance petrological and geochemical techniques. Notably, the associated black shale partings have received limited research attention (Singh et al. 2020), regarding their source rock characterization and hydrocarbon generation potential. The preliminary study suggested that the black shale deposits in the Palana Formation contain mainly hydrogen-rich Types I and II kerogen, which are thermally immature organic matter and with excellent potential for oil generation potential (Singh et al. 2020).

Preprints (www.preprints.org) | NOT PEER-REVIEWED | Posted: 24 November 2023 doi:10.20944/preprints202311.1550.v1

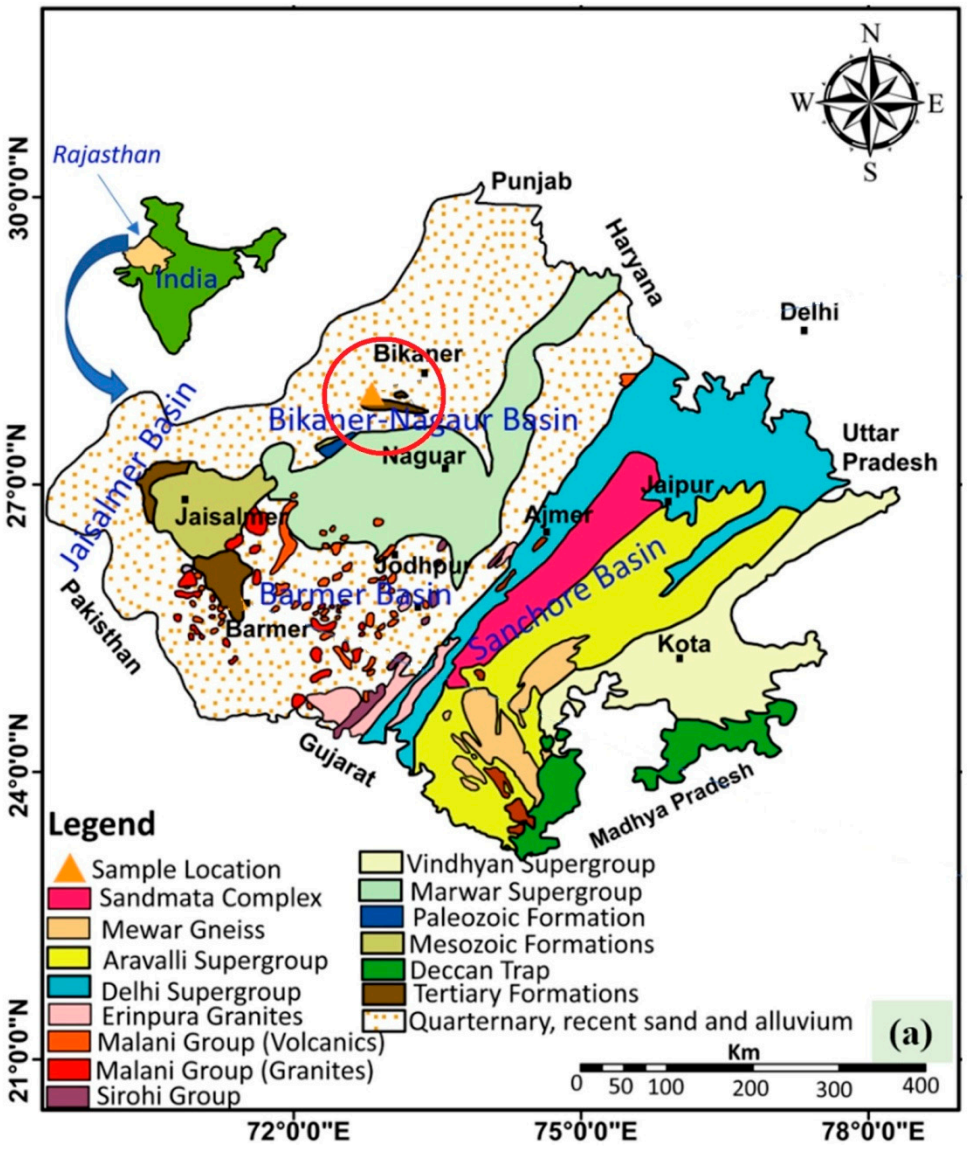

Figure 1. Geological map of Rajasthan showing the Gurha mine location in the Bikaner Nagaur Basin, northwestern India.

Although previous geochemical assessments are focusing on the organic matter in the black shale facies within the Palana Formation and its potential for hydrocarbon generation (Singh et al. 2020), the questions about the influence of the depositional environment factors and the reasons for the high of organic carbon accumulation in the black shale rocks of the Palana Formation remain largely unclear.

The main objective of the current research is devoted to understand the source of organic matter (OM), depositional environment factors (i.e., upwelling, reducing, and warm climatic conditions) and volcanogenic factors that influenced the high bioproductivity and organic carbon accumulation in the black shale rocks of the Palana Formation. In this case, the current study was integrated previously published data from bulk organic geochemistry with new findings from lithotype and mineral composition together with petrographical and geochemical characteristics of the black shale samples of the Palana Formation from the Gurha mine in the Bikaner-Nagaur Basin, western Rajasthan (Figure 1) using multi-techniques, including total organic carbon (TOC) and sulfur contents, kerogen microscopy, quantitative evaluation mineral-scanning electron microscopy

(QEMSCAN), X-ray diffraction (XRD), X-ray fluorescence (XRF), scanning electron microscope (SEM) analyses.

2. Geological Setting

Rajasthan, which includes the Thar Desert in the northwest, is the largest state in India, accounting for 10.75% of the country's total land area (Roy and Jakhar 2002). The state resides on the old earth's crust characterized by various geological and tectonic events (Shukla et al. 2023). The western region of Rajasthan has evolved through Cretaceous and Jurassic tectonic events. The separation of the Indian plate from the Gondwana supercontinent during the Jurassic–Cretaceous era led to the formation of a rift basin in western Rajasthan and initiated the geological development of the region (Singh and Kumar 2017; Shukla et al. 2023).

In the Rajasthan, three different sedimentary basins, including the Bikaner-Nagaur, Barmer, and Jaisalmer Basins were developed due to the intracratonic sedimentation, with an area of approximately 120,000 km2 (Bhowmick 2008). However, multiple phases of volcanic rock sequences and metasediment cycles occurred during the Precambrian in Rajasthan. These phases jcombined to form a banded gneiss structure that acts as the basement rock. These oldest basement gneiss rocks of the Archean age are collectively known as the Banded Gneissic Complex.

The sedimentary basins of Rajasthan comprise tectonic and lithological units spanning the Archean to Recent eras (Figure 1). The lithostratigraphic column and of the Bikaner-Nagaur Basin is presented in Figure 2. This basin contains a mixture of clastic, and carbonate sediments ranging from the Paleozoic (Cambrian-Permian) to the Cenozoic (Paleocene-Pliocene) era, as well as the Recent age (Figure 2). The Cambrian Nagaur Formation is the deepest sedimentary succession in the Bikaner-Nagaur Basin, which lies unconformably on the Precambrian basement rocks (Figure 2). The Cambrian Nagaur Formation comprises siltstone, brick red clay stone, and sandstone with clay bands (Figure 2). The Nagaur Formation, unconformably overlain by the Bap beds, consists of phyllite, gneiss, quartzite, pebbles and cobbles. Tertiary sediments are found in conformable contacts, such as the Jogira Formation, Marth Formation, and Palana Formations. The detailed lithological sequence of the Tertiary formations is illustrated in Figure 2. However, the Paleocene-Eocene Palana Formation is the primary subject of this investigation, which is composed of mainly lignite with carbonaceous and black shale (Figure 2). The lignite-bearing Palana Formation in the Bikaner-Nagaur Basin includes land-derived spores-pollen assemblages, showing that the floristic linkage was tropical to subtropical and influenced by humid climatic conditions during peat accumulation (Mathews et al., 2020). The presence of flora assemblages in the Palana lignite and shale sediments is also suggests the presence of a mixed (rainforest/ semi-arid/tropical evergreen) climatic condition in and around the mine area (Shukla and Mehrotra, 2014, 2016, 2018). The presence of the paralic environment under suboxic-anoxic character (reducing conditions) was enough for accumulation and enhancement the growth of algae and other microorganisms in the black shale of the Palana Formation (Mathews et al., 2020; Singh et al., 2020).

 doi:10.20944/preprints202311.1550.v1

Age	Formation	Lithology	
Recent & sub recent	---------	Blown sand	
Eocene to Paleocene	Jogira Marth Palana	Fossiliferous marl, fullers earth, clayey marl Ferruginous sandstone, gritty sandstone, siltstone Carbonaceous and black shale, lignite, fullers earth	
----------*unconformity*----------			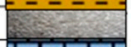
Early Permian	Badhaura	Medium to coarse grained ferruginous sandstone, clays, shale and siltstone	
----------*Unconformity*----------			
Early Carboniferous	Bap	Pebbles and cobbles, phyllite, slate, quartzite, gneiss, limestone	
----------*Unconformity*----------			
Cambrian	Nagaur	Brick-red claystone, siltstone, sandstone with caly band	
Precambrian	Malani Igneous suite	Malani rhyolites, tuffs, granites, porphyry, quartz veins and dykes	

Figure 2. Generalized stratigraphic column in Bikaner-Nagaur Basin, including igneous rocks and sedimentary sequence.

3. Materials and Methods

Nineteen black shale samples of the Paleocene-Eocene Palana Formation were collected from the exposed mine face of Gurha in the Bikaner-Nagaur Basin (Figure 3). The sampling method described by Schopf (1960) was followed during the sample collection from bottom to top. However, these black shale samples were subjected to multi-geochemical and petrological analyses as highlighted in the next subsections.

Preprints (www.preprints.org) | NOT PEER-REVIEWED | Posted: 24 November 2023 doi:10.20944/preprints202311.1550.v1

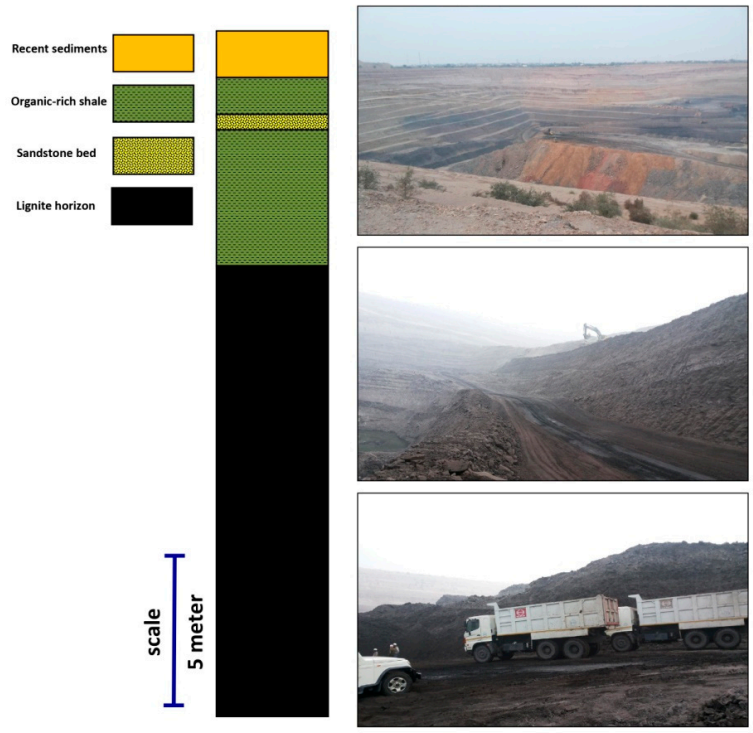

Figure 3. Lithology of the studied Gurha mine section, including the studied black shale horizons and their photographs of the outcrop section .

3.1. Geochemical Analyses

Several geochemical measurements of TOC and S contents were carried out on the studied black shale samples of the Palana Formation from Gurha mine in the Bikaner-Nagaur Basin (Table 1). The collected samples were milled into 72-mesh size using a mortar and pestle and used for TOC and S content measurements. However, the preliminary geochemical results of TOC and S contents for most of the studied Palana shale samples (14 samples) are available from our prior published research by Singh et al. (2020), and the other new 5 samples are added in the current study.

Table 1

Geochemical results of the of the analyzed black shales of the Paleocene-Eocene Palana Formation in western Rajasthan, India, including Total organic carbon (TOC) and total sulfur (TS) contents and bulk mineral compositions from XRD analysis

Basin	Mine	Samples ID	TOC Wt.%	TS Wt.%	Bulk mineral compositions (XRD results)													
					Silica minerals						Clay minerals					Carbonate minerals		
					Quartz	Olivine	Apophyllite	Tridymite	Albite	Total	Kaolinite	Dickite	Muscovite	Zeolite	Total	Calcite	Cerussite	Total
Bikaner-Nagaur Basin	Gurha	BSG-1	21.75	1.90														
		BSG-2	30.69	1.80														
		BSG-3	29.75	2.10														
		BSG-4	32.40	1.90														
		BSG-5	29.41	1.70														
		BSG-6	18.23	2.18	11.7	11.7		7.8		31.2	14.7	11.8		2.0	33.4		1.0	1.0
		BSG-7	25.26	1.70	16.0	25.0				41.0	19.0			4.0	23.0	3.0	2.0	5.0
		BSG-8	30.30	1.84														
		BSG-9	31.08	1.79	4.0	29.3	13.1	7.1		53.5	27.3	19.2			46.5			
		BSG-10	30.04	2.04	9.0	29.0		7.0		25.0	8.0	21.0	15.0	2.0	51.0	2.0	1.0	3.0
		BSG-11	29.46	2.24	3.9	30.4		8.8		43.1	22.5	19.6		2.0	44.1		2.0	2.0
		BSG-12	28.57	2.12														
		BSG-13	36.23	1.72	13.0	23.0	8.0	11.0		55.0	24.0	17.0		2.0	43.0			
		BSG-14	26.73	1.63	2.0	32.4			9.1	43.5	14.1		16.2	6.1	36.4		1.0	1.0
		BSG-15	32.09	1.55	10.8					10.8	21.6	15.7	19.6	2.9	59.8	2.9		2.9
		BSG-16	28.64	1.85														
		BSG-17	33.04	1.74	19.8	5.0		5.9		30.7	15.8	11.9		3.0	30.7		1.0	1.0
		BSG-18	29.57	2.09														
		BSG-19	4.04	1.91	42.0	2.0	3.0	5.0		52.0	5.0	6.0		1.0	12.0		1.0	1.0

Basin	Mine	Samples ID	Bulk mineral compositions (XRD results)									
			Heavy minerals						Other minerals			
			Anatase	Zircon	Clinopyroxene	Ilmenite	Rutile	Total	Gypsum	Apatite	Pyrite	Total
Bikaner-Nagaur Basin	Gurha	BSG-1										
		BSG-2										
		BSG-3										
		BSG-4										
		BSG-5										
		BSG-6	1.0	2.0	3.9	2.0		8.9	19.6		2.9	22.5
		BSG-7	3.0	4.0	7.0		2.0	16.0	7.0	8.0		15.0
		BSG-8										
		BSG-9										
		BSG-10		2.0	7.0			9.0	4.0	4.0	4.0	12.0
		BSG-11	2.9					2.9			7.8	7.8
		BSG-12										
		BSG-13	2.0					2.0				
		BSG-14	2.0	1.0		2.0	3.0	8.0				
		BSG-15	3.9	2.9	12.7			19.5	6.9			6.9
		BSG-16										
		BSG-17							13.9	20.8		34.7
		BSG-18										
		BSG-19	1.0		4.0	1.0		6.0	24.0	4.0	2.0	30.0

doi:10.20944/preprints202311.1550.v1

 doi:10.20944/preprints202311.1550.v1

3.2. Optical-Microscopic Examinations

In this study, optical-microscopic examinations were conducted on the whole rocks using a standard polished block method using a reflected light microscope (Taylor et al., 1998).

The collected samples were milled into ±18 mesh (approximate ≤1mm) sizes using a mortar and pestle. For embedding the shale particulates mounts, epoxy resin, an epoxy hardener, a release agent, and sample cups were used. The shale pellets were ground for 3-5 min with a polishing machine using different silicon carbide waterproof (papers (mesh size: 180, 320, 600, 800, 1000, 1200, and 2000; speed: 150-180 RPM) under continuous slow water flow. Buehler MicroCloth and MicroPolish gel (0.05 micron) were used to polish the pellets. The polished blocks were then immersed in oil and studied under white reflected light and cross-polarized under UV light with a LEICA microscope (model DM6000M) which had fluorescence illumination capabilities, which enabled examination of the organic facies and differentiation of its assemblages.

3.3. Mineralogical and Elemental Compositions Analyses

Various techniques are utilized to investigate the geochemical and mineralogical compositions, including both bulk and surface analyses using different types of samples.

The bulk analysis is conducted using X-ray Fluorescence (XRF) and X-ray diffraction (XRD) techniques, which uses X-rays to provide information about the overall composition of the samples. In this case, ten black shale samples were crushed to less than 200 meshes and studied by X-ray fluorescence (XRF) spectrometer using PANalytical (EPSOLON3X) XRF spectrometer. The XRF analysis was used to determine the concentrations of the major oxides and trace elements in the studied black shale samples.

Additionally, the bulk mineralogy of the targeted samples is investigated using X-ray diffraction (XRD) of the Malvern PANalytical EMPYREAN Diffractometer system at two theta ranges of 2-70 and 0.01 step size. The acquired XRD data are processed using X'Pert Highscore software. Qian et al. (2015) and Amao et al. (2022) illustrated and discussed the concepts and experimental design of such a technique.

For surface analysis, three polished shale samples were subjected to obtain more detailed information about the mineralogical and geochemical composition of specific spots by scanning electron microscopy (QEMSCAN), including species identification (SPI), scanning electron microscopy (SEM) and Energy Dispersive Spectroscopy (EDS). However, the QEMSCAN analysis is used to scan the sample with an electron beam and analyze the backscattered electrons to determine the mineralogical and geochemical composition of selected spots. The concepts, workflow, and applications of QEMSCAN are discussed in the literature, including Ayling et al. (2012), Qian et al. (2015), and Alqubalee et al. (2021).

4. Results

4.1. Total Organic Carbon (TOC) and Sulfur (S) Contents

The presence of organic matter richness in the sediments commonly infers by the organic carbon content (TOC), which is conventionally reported as a function of weight percent (Bissada 1982; Jarvie, 1991; Peters, 1986; Katz and Lin 2014). In this regard, the studied black shales of the Paleocene-Eocene Palana Formation are enriched by organic matter with high TOCs range between 4.04-36.23 wt. percent (Table 1). Most of the measurements indicate TOC > 10 wt. % (18.23 %–36.23 %), while one sample exhibits TOC of 4.04 % as shown in Table 1. The high amount of the organic matter points towards a reducing environmental condition during deposition of these studied black shale sediments. However, the assessment of the reducing environmental conditions using other geochemical data, which are detailed in the following sections.

In addition, the sulfur content in the studied shale samples was measured and ranges from 1.55 wt% to 2.24 wt% (Table 1). The S content usually differentiates marine environments from non-marine (Berner and Raiswell, 1983). A high S content of > 1 wt.% denotes a marine environment

Preprints (www.preprints.org) | NOT PEER-REVIEWED | Posted: 24 November 2023 doi:10.20944/preprints202311.1550.v1

(Berner and Raiswell, 1983; Hakimi et al., 2016), which has been the case for the Palana black shale facies. However, the relationship between TOC and S contents also agrees that the analyzed black shales generally fall within the normal marine environmental setting (Figure 4).

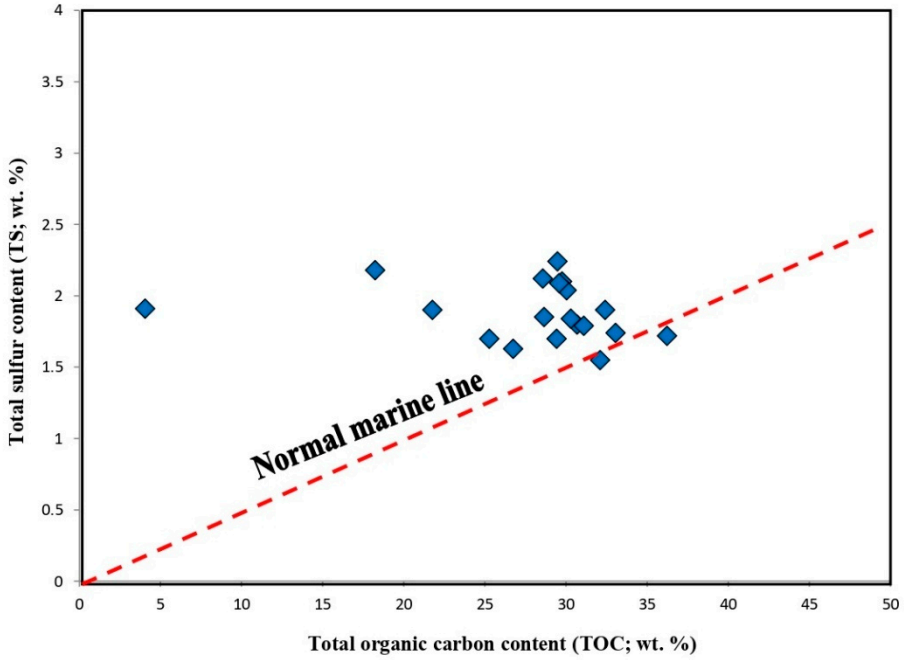

Figure 4. Relationship between TOC and TS content for the studied black shale samples of the Palana Formation, showing normal marine environmental setting.

4.2. Organic Facies Characteristics

Organofacies in the studied black shale samples of the Palana Formation in the Gurha (Bikaner-Nagaur Basin) were identified using microscopic investigation under UV radiation reflected light as shown in Figure 5. The organofacies are dominated by high amounts of liptinite, with small amounts of huminite maceral from the terrestrial organic matter (Figure 5). The liptinite maceral in the studied shale samples are presented as structured and unstructured organic matter, including alginate, sporinite, and resinite, which are characterized by fluorescence emission colours ranging from orange to yellow (Figure 5). However, the hydrogen-rich liptinites display a high abundance of the alginate, and they were classified into telalginite and lamalginite based on their morphologies (Figure 5a–e). telalginite arises from algae and occurs as fan-shaped, flattened discs and discrete lenses (Figure 5a and b), whereas Lamalginite occurs as thick lamellae (Figure 5c–e). In addition, most of the sporinites in the black shale samples occur as thin wall isolated microspores (Figure 5e,f). Other unstructured macerals such as resinite also occurred in the studied shale samples (Figure 5). The resinite appears as rounded, oval, and laminar shaped (Figure 5g,h).

Preprints (www.preprints.org) | NOT PEER-REVIEWED | Posted: 24 November 2023 doi:10.20944/preprints202311.1550.v1

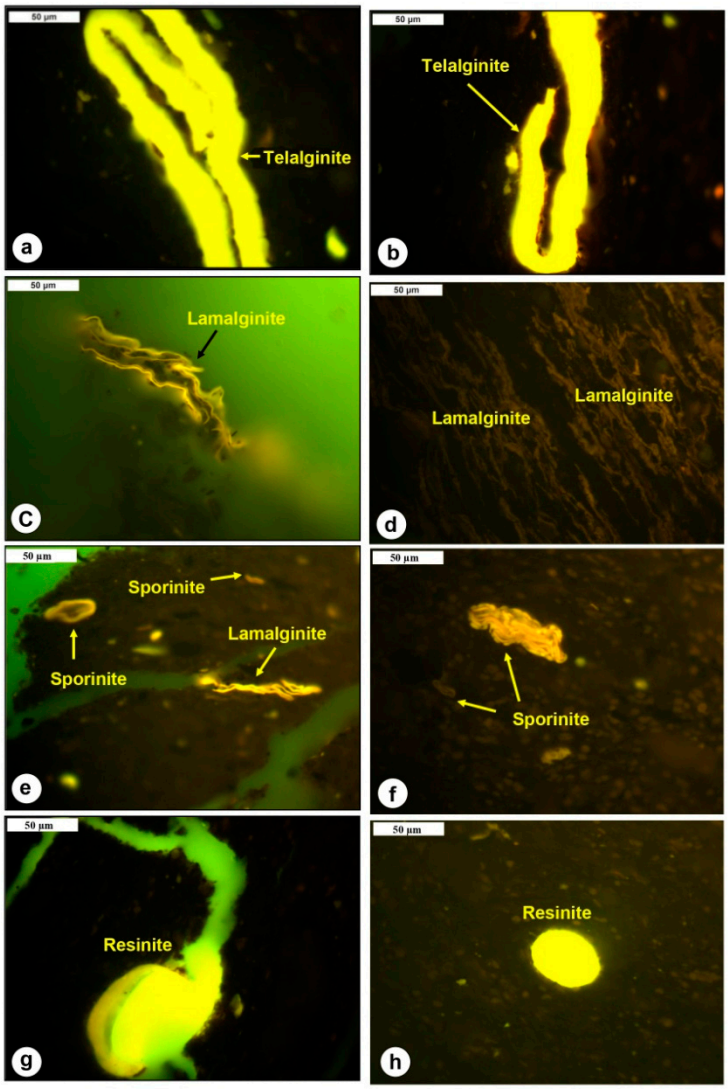

Figure 5. Photomicrographs of the studied black shale samples of the Palana Formation, under reflected UV light, with a field width of 0.2 mm, including different organic matter assemblages of liptinite such as alginite, sporinite and resinite.

4.3. Mineralogical Composition and Lithotype

In this research, the bulk mineral compositions of the analyzed black shale samples from the Palana Formation were primary demonstrated by the XRD result couple with QEMSCAN results for the surface of the samples. According to the mineral composition distributions in the XRD results, the clay (12.41%–59.8%) and silica (10.8%–55.0%) minerals prevails over the carbonate minerals (1%–5%), with significant amounts of heavy minerals (2.0%–19.5%), and other minerals (6.9%–34.7%), including gypsum, apatite and pyrite (Table 1). Most of the clay minerals of the Palana black shale samples are kaolinite, dickite, with muscovite and some of zeolite, while the silica minerals comprise of quartz, olivine and some different silica minerals (i.e., apophyllite, tridymite, and albite). However, the prevalence of clay (12.41%–59.8%) and silica (10.8%–55.0%) minerals in the Palana black shale samples is inferred as mainly clay-rich siliceous mudstone lithotype with silica-rich argillaceous mudstone and silica dominated lithotype (Figure 6).

Preprints (www.preprints.org) | NOT PEER-REVIEWED | Posted: 24 November 2023 doi:10.20944/preprints202311.1550.v1

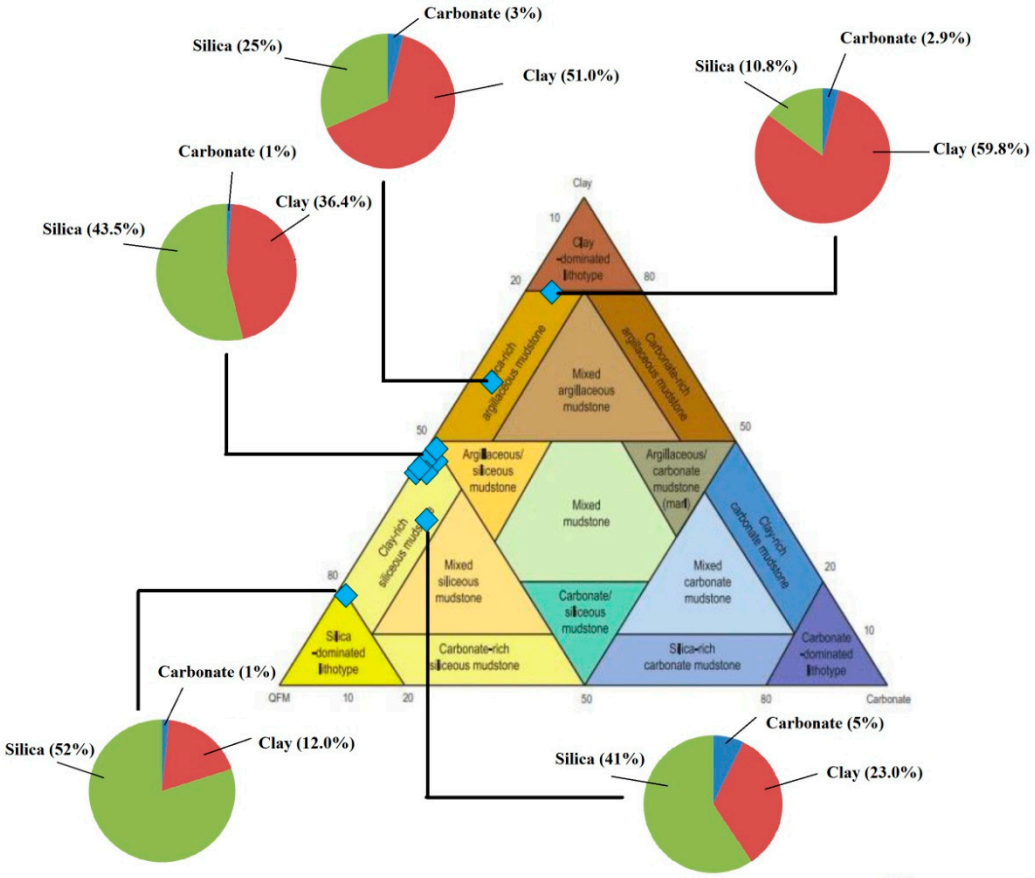

Figure 6. Ternary plot of the comparison of silica, carbonate, and clay content showing lithology types of the studied black shale samples of the Palana Formation.

Such enrichment in clay with quartz minerals, particularly kaolinite with chlorite is also clearly demonstrated from the species identification (SPI) of the QEMSCAN results (Figure 7). The QEMSCAN results also deciphered that the Palana shale facies contains mainly organic matter associated with other minerals such as siderite, gypsum and pyrite and heavy minerals (Figure 7). In addition, the SEM results also reveal that the analyzed Palana shale samples contain high clay minerals (Figure 8A), including kaolinite, dickite and chlorite (Figure 8A1,2). The presence of barite mineral was also obtained using SEM (Figure 8B), and show that the major white fabric barite was observed in the studied samples (Figure 8B1), and associated with organic matter (Figure 8B2,3), and pyrite mineral, with the form of the framboid pyrite (Figure 8D1). The occurrence of the foraminifera assemblages in the studied samples (Figure 8D2) suggests marine environment setting. This finding of the marine setting also demonstrated by the presence of the coccolithophore plankton (Figure 9A), which is regarded as marine algae. However, the SEM also shows the fabric barite mineral mainly associated with algal-and bacterial- derived organic matter (Figure 9B,C). From this point of view, the presence of barite mineral in the studied shale samples is may formed as replacement of the gypsum mineral due to the bacterial mediation in a humid climate (Forjanes et al., 2020; Ruiz et al., 2020).

Preprints (www.preprints.org) | NOT PEER-REVIEWED | Posted: 24 November 2023 doi:10.20944/preprints202311.1550.v1

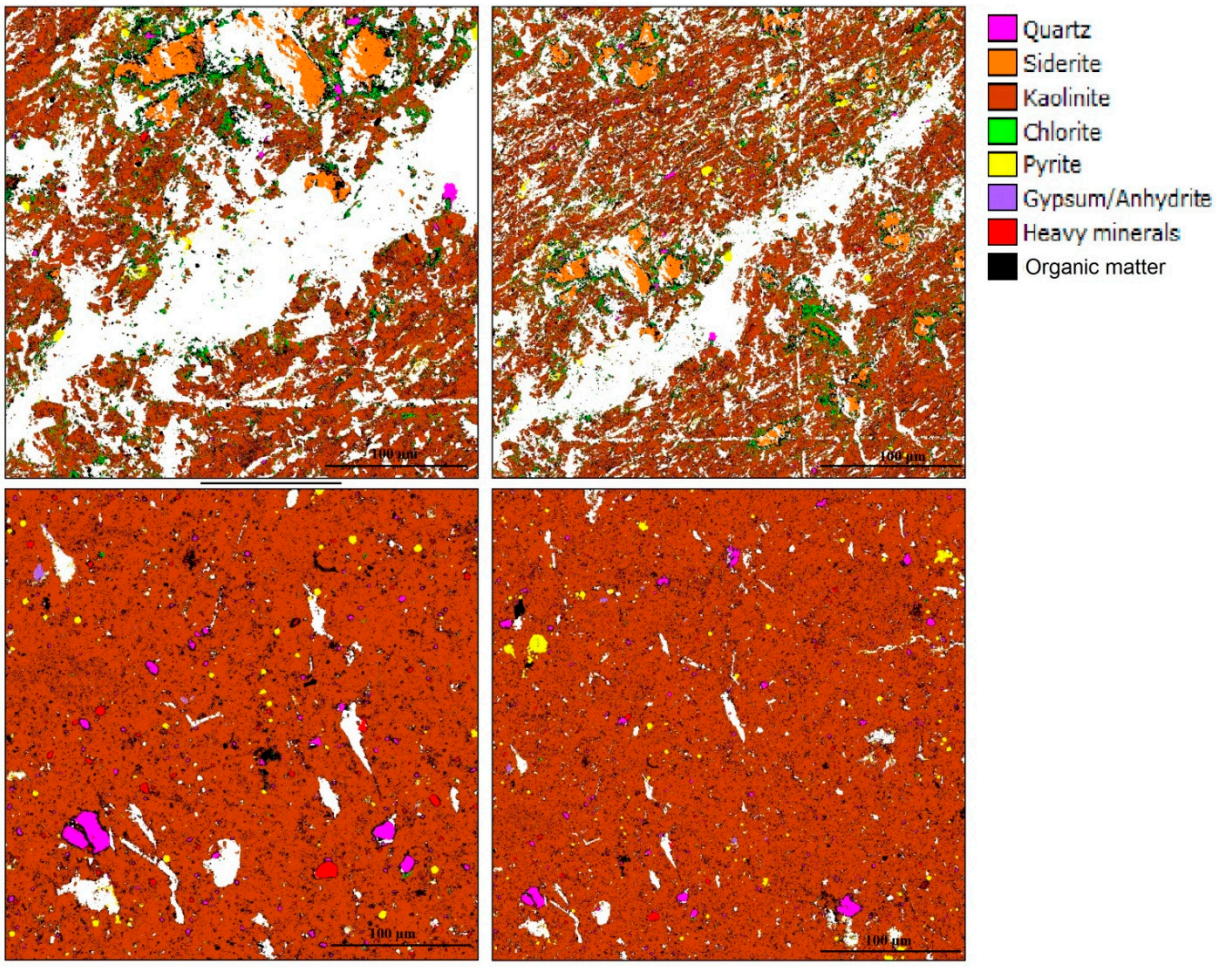

Figure 7. QEMSCAN image showing the mineral compositions and associated organic matter in the studied black shale samples of the Palana Formation.

Preprints (www.preprints.org) | NOT PEER-REVIEWED | Posted: 24 November 2023 doi:10.20944/preprints202311.1550.v1

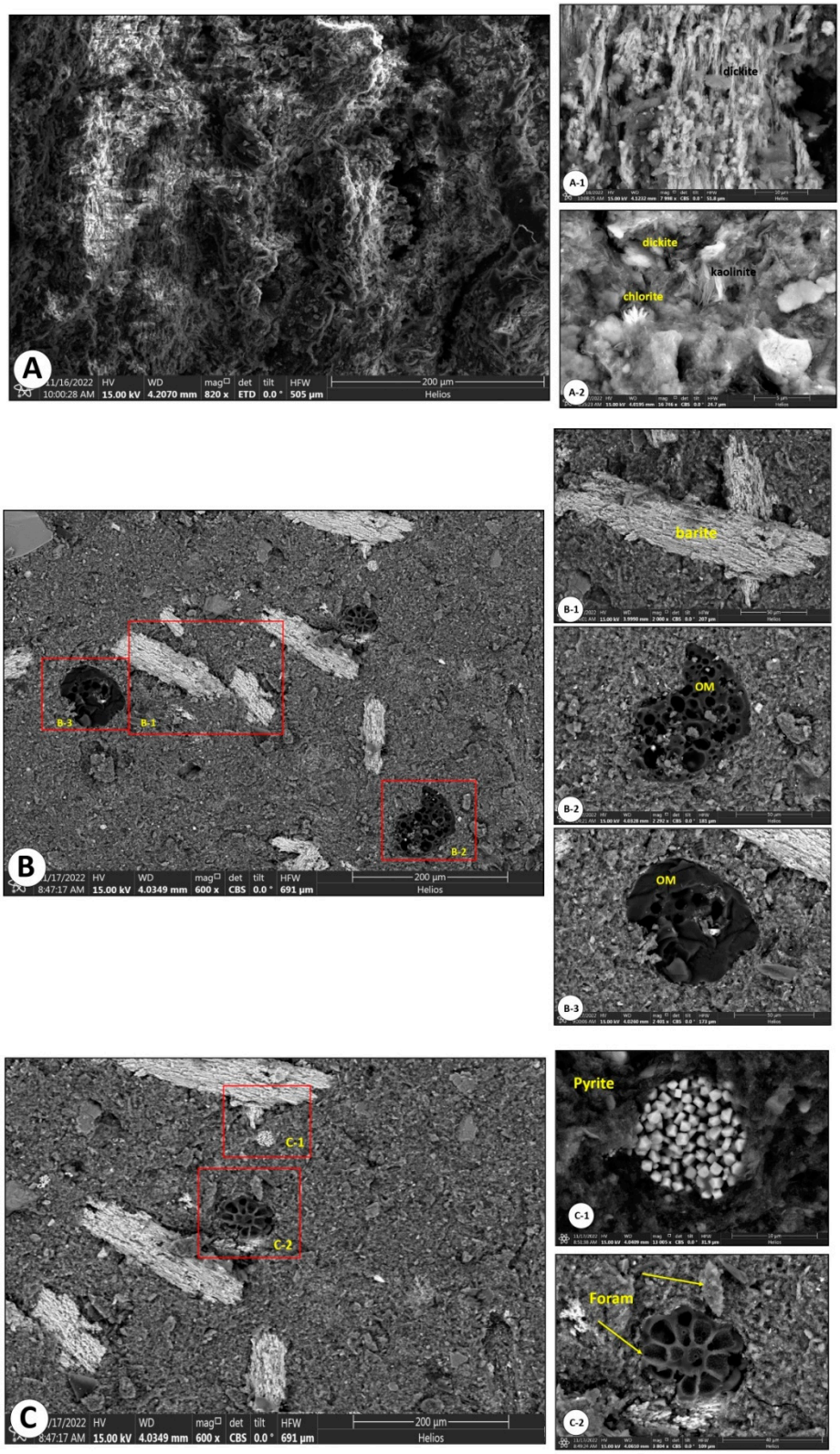

Figure 8. Photomicrographs of the SEM for the mineral composition and associated organic matter in the studied black shale samples of the Palana Formation.

Preprints (www.preprints.org) | NOT PEER-REVIEWED | Posted: 24 November 2023 doi:10.20944/preprints202311.1550.v1

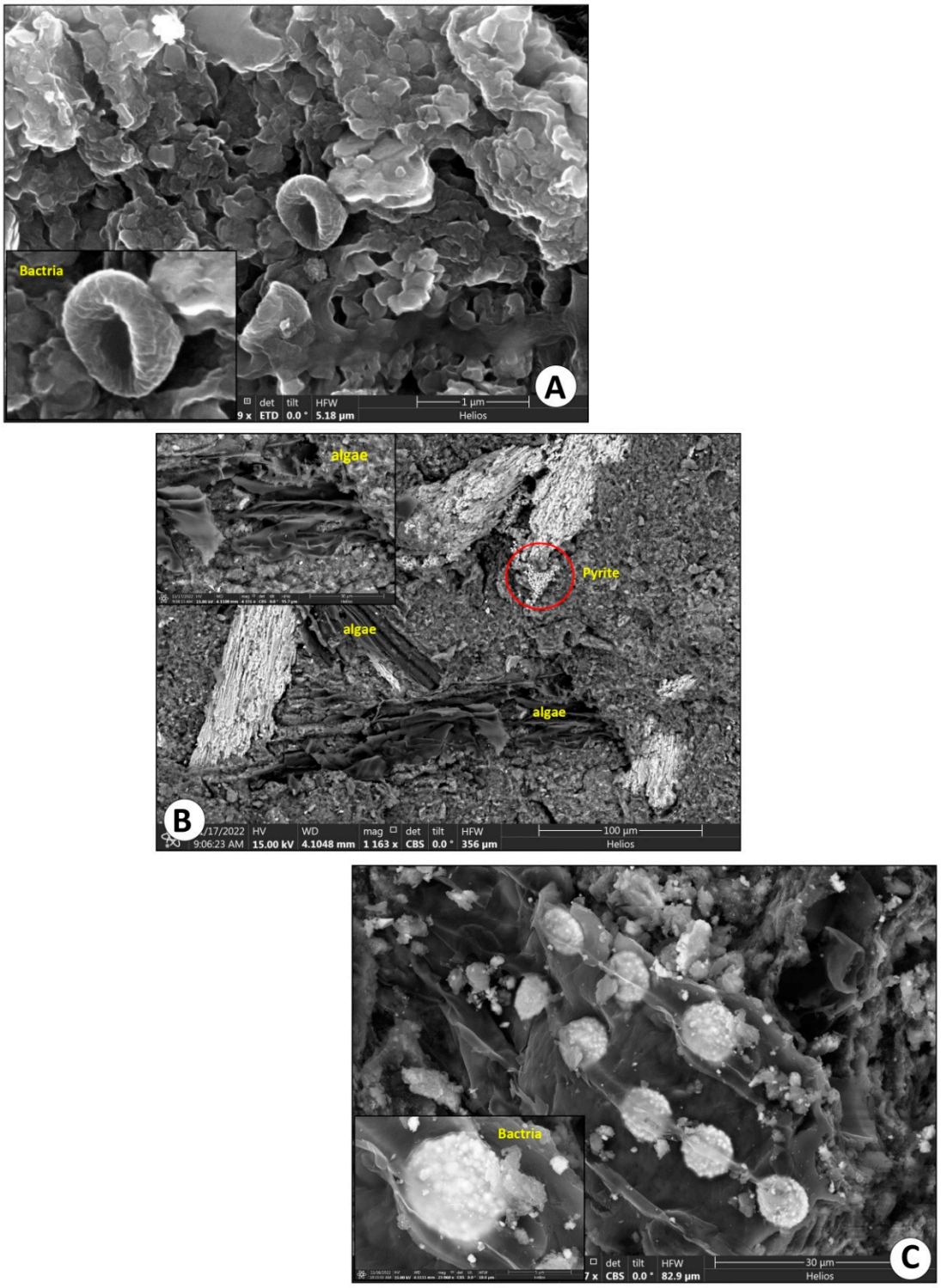

Figure 9. Photomicrographs of the SEM for the most organic matter input in the studied black shale samples of the Palana Formation.

4.4. Major Oxides and Trace Elements

The abundances of major oxides and selected trace elements as well as their ratios are given in Table 2. Most of the studied Palana shale samples are higher in SiO2 (42.49-51.69 wt %), Al2O3 (26.68-

Preprints (www.preprints.org) | NOT PEER-REVIEWED | Posted: 24 November 2023 doi:10.20944/preprints202311.1550.v1

32.22 wt %), and significant amounts of Fe2O3 (8.61-22.68 wt %), while they are depleted in TiO2, SO3, CaO, MgO, P2O5, Na2O and K2O, respectively (Table 2).

The correlation between the Fe2O3 and SO3, as indicated by the cross-plot Fe-S show that the high concentrations of the Fe2O3 in most of the samples plotted to the right of the line defined by pyrite (Figure 10a), suggesting the pyrite is not the main source of the significant of Fe fraction in the analyzed samples and come from other sources like olivine mineral. The XRD results confirm that significant amounts of olivine are present in the analyzed shale samples (Table 1); thus, olivine is the main source of Fe, as clearly demonstrated by the direct proportional between the Fe2O3 and olivine mineral, as shown in Figure 10b.

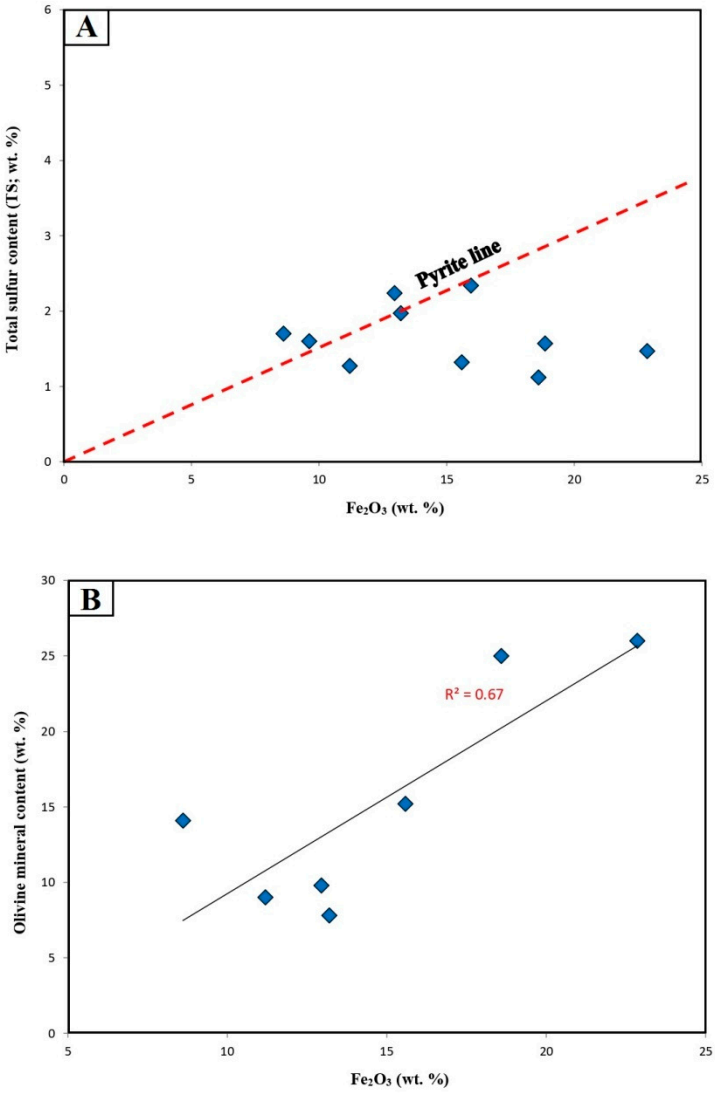

Figure 10. (A) Relationship between F2O3 and TS content, and (B) F2O3 versus olivine mineral content of the studied black shale samples of the Palana Formation, showing that the Fe element mainly sourced from olivine.

Table 2

Inorganic geochemical data (X-ray fluorescence analysis), including major oxides (%) and trace elements (ppm) of the analyzed black shales of the Paleocene-Eocene Palana Formation in western Rajasthan, India

Sample ID	Major oxides (%)																	
	SiO_2	Al_2O_3	CaO	Fe_2O_3	K_2O	MgO	P_2O_5	TiO_2	Na_2O	SO_3	MnO	Al/K	K/Al	Ca/Mg	Fe+Mn/Ti	100*Mg/Al	CIA	PIA
BSG-6	46.58	31.31	1.45	13.20	0.12	0.46	0.25	3.64	0.24	1.97	0.01	260.9	0.004	3.15	13.20	1.47	94.54	94.90
BSG-7	43.44	30.22	1.40	18.59	0.08	0.47	0.40	3.71		1.12	0.02	377.8	0.003	2.98	18.60	1.56	95.33	95.58
BSG-9	51.69	31.23	1.41	15.95	0.27	0.74	0.14	3.30	0.30	1.70	0.01	115.7	0.009	1.91	8.61	2.37	94.04	94.85
BSG-10	43.40	26.68	1.14	22.86	0.18	0.61	0.22	2.61	0.27	1.47	0.02	148.2	0.007	1.87	22.87	2.29	94.38	95.01
BSG-11	46.53	31.27	1.63	12.95	0.10	0.51	0.29	3.48	0.24	2.24	0.01	312.7	0.003	3.20	12.95	1.63	94.07	94.37
BSG-13	48.48	30.22	1.45	11.20	0.19	0.40	0.28	3.14	0.24	1.27	0.02	159.1	0.006	3.88	11.21	1.32	94.14	94.74
BSG-14	42.49	32.22	1.60	15.59	0.09	0.57	0.50	3.51	0.33	1.32	0.02	358.0	0.003	2.81	15.60	1.77	94.10	94.36
BSG-15	50.79	31.23	1.51	9.61	0.29	0.78	0.19	2.80	0.39	1.60	0.01	107.7	0.009	1.94	9.61	2.50	93.45	94.31
BSG-17	45.90	29.65	1.24	18.86	0.22	0.69	0.32	2.91	0.29	1.57	0.02	134.8	0.007	1.80	18.87	2.33	94.43	95.13
BSG-19	49.83	28.27	1.23	8.61	0.08	0.61	0.31	3.18	0.26	2.34	0.01	353.4	0.003	2.51	15.95	2.16	94.74	95.01

Trace elements (ppm)																		
V	Cr	Co	Ni	Cu	Zn	Ga	Rb	Sr	Zr	Cd	Ba	Rb/Sr	V/Ni	V/V+Ni	V/Cr	Sr/Cu	Sr/Ba	Ga/Rb	Co*Mn
1690	637.9	588.4	233.3	497.1	199.9	68.6	6.8	380.1	830.8	9.2	166.1	0.02	7.24	0.88	2.65	0.76	2.29	10.09	0.0006
1660	647.8		258.7	438.6	154.6			582.4	825.8				6.42	0.87	2.56	1.33			
1550	590.5	391.3	220.2	435.5	292.0	73.2	21.7	347.5	786.4	39.6	206.2	0.06	7.04	0.88	2.62	0.80	1.69	3.37	0.0004
1090	470.9	1050	139.8	312.3	180.2	46	15.6	276.7	606.5	26.0		0.06	7.80	0.89	2.31	0.89		2.95	0.0021
1620	628.3	596.3	247.0	502.5	226.5	73.3	7.3	509.1	782.2	27.3	233.2	0.01	6.56	0.87	2.58	1.01	2.18	10.04	0.0006
1590	537.6	598.4	223.3	397.1	299.9	68.6	7.8	280.1	850.8	28.8	186.1	0.03	7.12	0.88	2.96	0.71	1.51	8.79	0.0012
1060	447.8	578.4	368.7	438.6	184.6	78.0	13.7	592.4	725.9	20.7	210.8	0.02	2.87	0.74	2.37	1.35	2.81	5.69	0.0012
1650	580.4	491.3	240.5	415.5	299.8	65.2	23.7	357.5	656.4	35.6	209.2	0.07	6.86	0.87	2.84	0.86	1.71	2.75	0.0005
1190	570.8	1090	159.2	212.3	150.5	46.0	17.6	256.7	696.5	29.5	143.2	0.07	7.47	0.88	2.08	1.21	1.79	2.61	0.0022
1520	648.3	496.3	217.5	509.5	236.9	35.3	10.3	518.1	882.1	9.2	243.2	0.02	6.99	0.87	2.34	1.02	2.13	3.43	0.0005

CIA-= **Chemical index of alteration= [Al_2O_3*100/(Al_2O_3+CaO+Na_2O+K_2O)]**
PIA-= **Plagioclase index of alteration = [(Al_2O_3+ K2O)/(Al_2O_3+CaO+Na_2O+K_2O)*100]**

doi:10.20944/preprints202311.1550.v1

 doi:10.20944/preprints202311.1550.v1

However, the presence of the Si, Al, Fe, Ti, S, Ca, Mg, Na, Mn, and K elements, with associated with organic carbon (C) is also supported by the EDS results of the studied black shale samples of the Palana Formation, as shown in Figure 11.

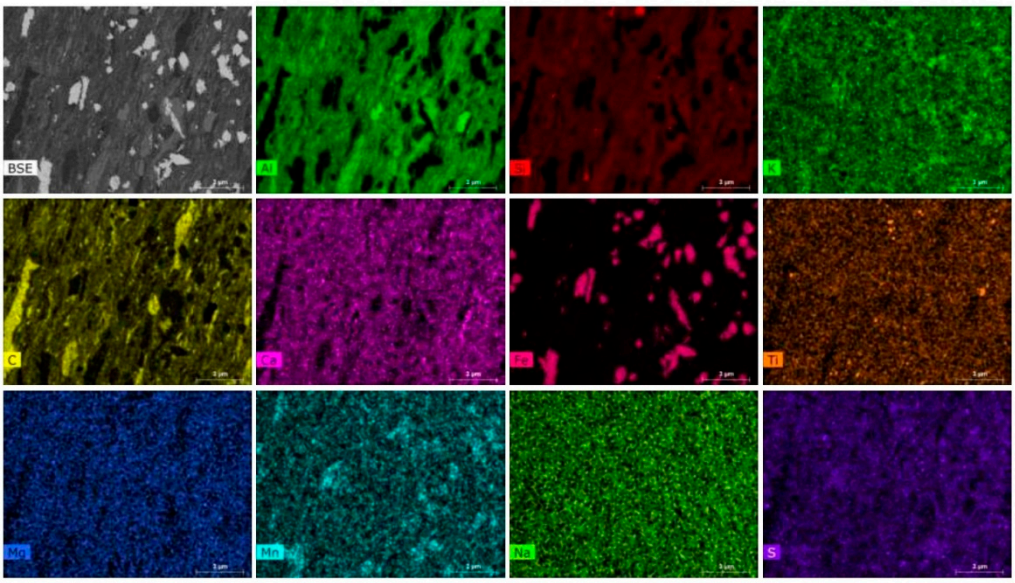

Figure 11. This figure also shows most of the major elements in the studied black shale samples of the Palana Formation using EDX spectra of the surface of sample.

Furthermore, the analyzed Palana shale samples show enrichment for V, Ni, Cr, Co, Cu, Zr, Zn, Sr and Ba trace elements (Table 2). The observed enrichment of trace elements in the studied samples, especially V, Ni, and Sr is suggestive of a brackish-water environment (Barwise, 1990).

The Palana samples also contain other trace elements in low amounts such as Ga, Cd, Rb, respectively (Table 2). However, several geochemical ratios such as V/Ni, V/(V+N), V/Cr, Sr/Cu, Sr/Ba and Ga/Rb were calculated based on the abundances of their trace elements and found to be in the range 2.87-7.80, 0.74-0.89, 2.08-2.96, 0.71-1.35, 1.51-2.81 and 2.61-10.09, respectively (Table 2). These ratios derived from trace elements are commonly used to assess the paleoredox and paleoclimate conditions, as discussed in the next subsections.

5. Discussion

5.1. Sedimentary Depositional Environment during the Paleocene-Eocene

The knowledge and information of the sedimentary depositional environment of the black shales of the Palana Formation during the Paleocene-Eocene were studied by employing multi proxies, including elemental data together with kerogen microscopy. In this case, the sedimentary depositional environments and their impact on organic matter accumulating in the black shale of the Palana Formation were discussed based on three main factors, including paleoredox conditions, paleosalinity and upwelling action.

The organic carbon accumulation and its preservation condition during deposition is directly linked to the paleoredox conditions (Katz, 2005; Zonneveld et al., 2010; Wei et al., 2023). The paleoredox conditions are divided into four levels based on the concentration of O2 in bottom water; namely oxic, dysoxic, anoxic non-sulfidic and anoxic sulfidic (euxinic) conditions.

In this study, anoxic condition (low oxygen) during the Paleocene-Eocene time was recognized based on the high amount of OM in the black shale facies of the Palana Formation, with TOC up to 36.23 wt. % (Table 1), which increased the effective preservation and resulted in the organic enrichment. The finding of the anoxic condition (low oxygen) during the Paleocene-Eocene time is

 doi:10.20944/preprints202311.1550.v1

established using redox-sensitive trace elements (i.e., Ni, V, Cr) and their ratios as redox proxies (Tribovillard et al., 2006).

The V and Ni trace elements are commonly insoluble and enrichment under the reducing environmental conditions, whereby can be used as redox-sensitive indicators for the anoxic environmental conditions (e.g., Bechtel et al., 2001; Algeo and Maynard, 2004; Tribovillard et al., 2006). In this case, the V element concentration is higher than Ni element in the black shale facies of the Palana Formation, indicating that marine anoxic environmental conditions is promoted during the Paleocene-Eocene, as indicated by the relationship between the V and Ni trace elements (Figure 12a). However, the anoxic environmental conditions during accumulation of the Palana black shale facies can also be determined by V/Ni and V(V+Ni) ratios (e.g., Galarraga et al., 2008; Hatch and Leventhal, 1992). The V/Ni ratio has been used by Galarraga et al. (2008) as an indicators for interpretation the paleoredox conditions. According to this work, V/Ni ratio of < 2 indicates an anoxic condition, while V/Ni ratio of >1 indicates deposition under oxic conditions. Generally, the values of V/Ni ratio recorded from the shale samples of the Palana Formation are higher than 2 (Table 2), further suggesting anoxic conditions during deposition of these shale sediments. Moreover, the V(V+Ni) ratio of the Palana shales under investigation is between 0.74 and 0.89, indicating anoxic environmental conditions during the deposition (Hatch and Leventhal, 1992). This interpretation is also demonstrated by the association between the V/(V+Ni) ratio and TS content, which alludes to the marine anoxic environmental conditions (Figure 12b).

In addition, the V/Cr ratio derived from trace elements are also commonly used to provide information of the oxygenation conditions in the environment of deposition (Jones and Manning, 1994). Jones and Manning (1994) suggested that the V/Cr ratio of higher than 4.5, anoxic conditions were predominant, while V/Cr ratio of less than 2 indications to oxic conditions. Accordingly, the values of the Palana shale samples are 2 < V/Cr < 4.5 (Table 2), resulting in anoxia with less prevalent during the period of their deposition. However, this study integrates the organic matter content and enrichment in some elements such as S and Fe and used to assess the environmental conditions during the deposition time, as reported by Algeo and Liu (2020). In this regard, the concentrations of Fe2O3 and S elements together with TOC content were plotted on Fe2O3-TOC-S ternary diagram and generally show that the Palana black shale samples plotted on the zone of low oxygen conditions (Figure 13). The anoxic depositional setting (low oxygen) of the Palana black shale facies during the Paleocene-Eocene was also recognized based the isoprenoid distributions and their narrow Pr/Ph ratio of less than 0.60 (Singh et al. (2020), which a low O2 conditions promote Ph enrichment when compared to Pr (Large and Gize, 1996).

Therefore, these anoxic environmental conditions during the Paleocene-Eocene contribute to preservation of organic matter and maximize the effect of organic carbon accumulation during deposition of the organic-rich shale sediments of the Palana Formation.

Preprints (www.preprints.org) | NOT PEER-REVIEWED | Posted: 24 November 2023 doi:10.20944/preprints202311.1550.v1

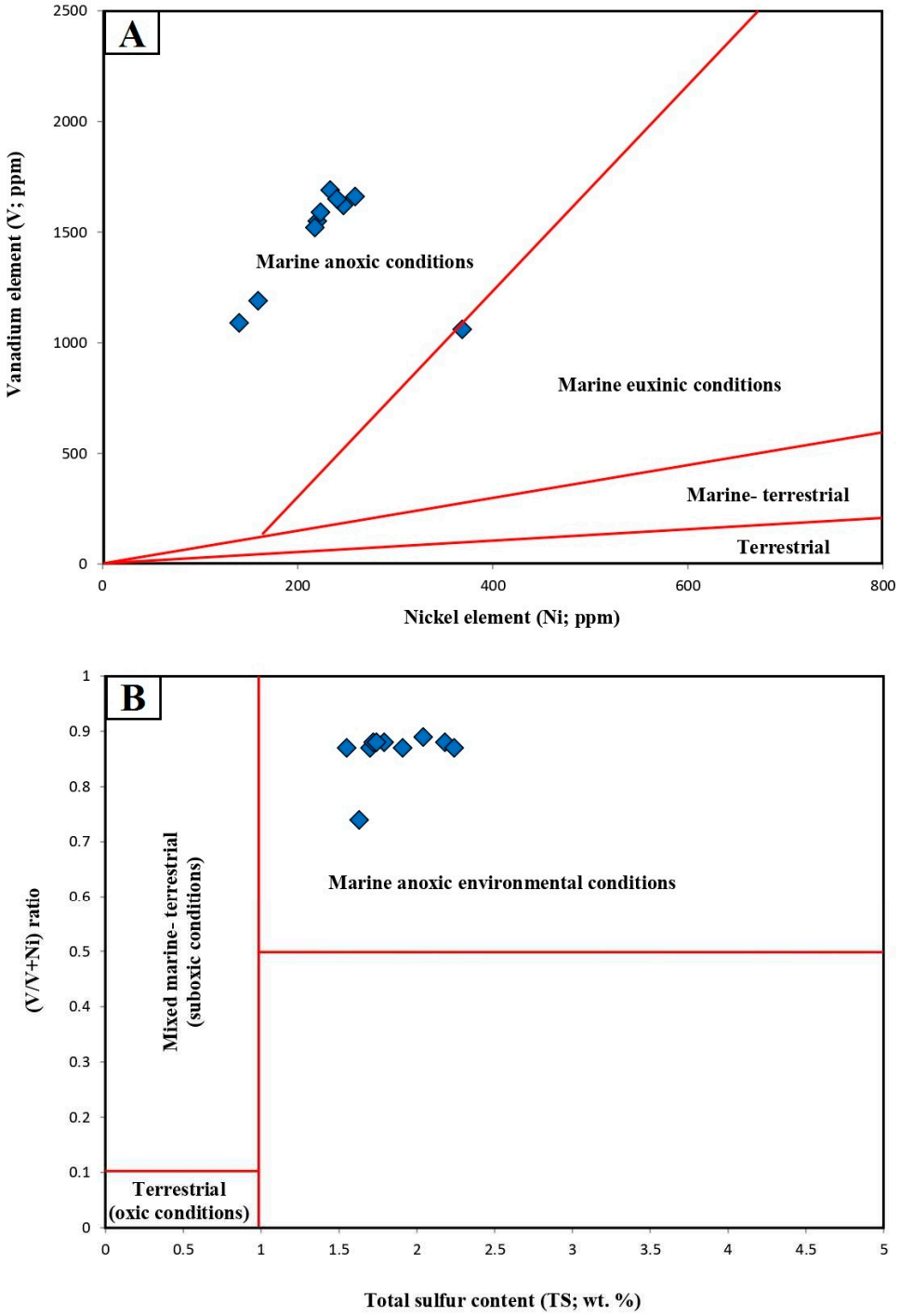

Figure 12. Geochemical correlations of (a) V and Ni trace elements and (B) total sulphur (TS) and V/(V+Ni) ratio, indicating highly marine reducing environmental conditions during deposition time (Paleocene-Eocene) in the studied black shale samples of the Palana Formation.

 doi:10.20944/preprints202311.1550.v1

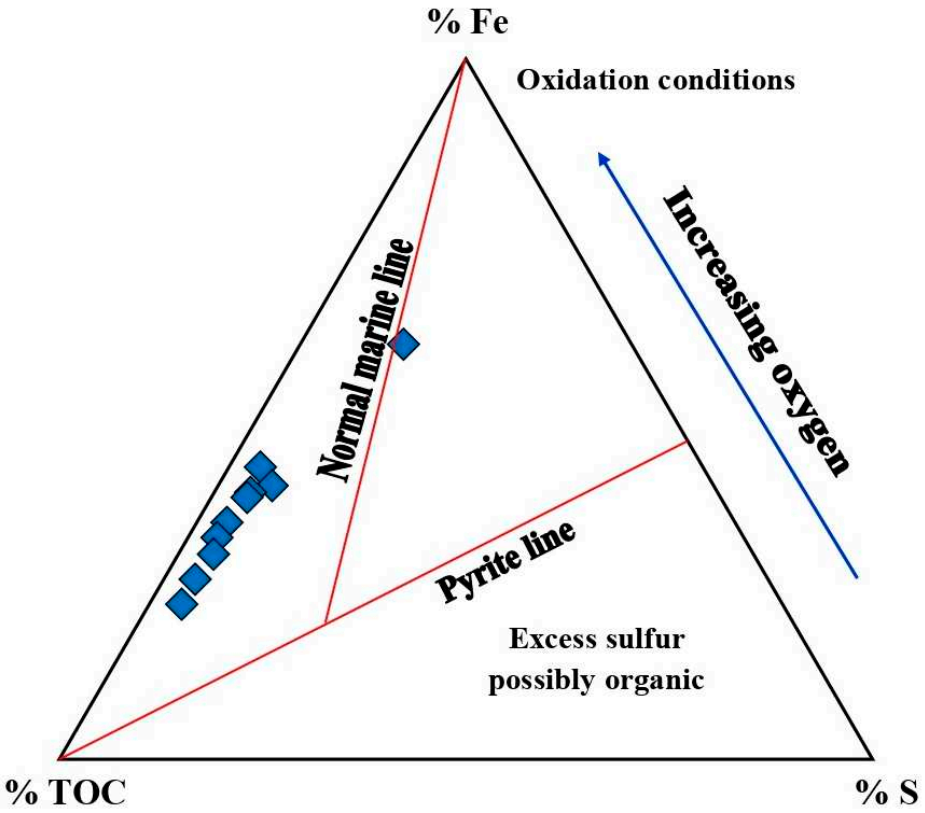

Figure 13. Ternary Fe2O3-TOC-S ternary diagram of the studied black shale samples of the Palana Formation, further showing low oxygen content (anoxic conditions) during deposition time (Paleocene-Eocene).

Furthermore, the reconstructing the paleosalinity conditions is other important factor and helpful for understanding the mechanism of the organic carbon enrichment, including the biological community and anoxic conditions of water column (Xu et al., 2015).

In this study, salinity-sensitive elements of the studied Palana black shale facies, including Ca, Mg and Al elements were used to assess the salinity degree during the Paleocene-Eocene depositional time (Wang et al., 2017; Orhan et al., 2019; Remírez and Algeo, 2020; Sun et al., 2022). In this regard, the Sr and Ba trace elements and their ratios of Sr/Ba (Table 2) are mainly used as an indicator for salinity and/or evaporation conditions (Read et al., 1995; Price, 1999; Vincent et al., 2006; Omar et al., 2020; Dashtgard et al., 2022). The high concentrations of Sr element can indicate for high salinity and/or evaporation conditions during the deposition of the sediments, with high values of the Sr/Ba ratio (Deng and Qian, 1993; Xu et al., 2015). Accordingly, the preliminary investigation of studied Palana black shale facies was deposited in moderate salinity stratification (brackish water), with relatively low Sr/Ba ratio between 1.51 and 2.81 (Table 2).

This finding is also consistent with the Sr/Ba ratio versus V/Ni ratio diagram, as the salinity stratification of the water columns regulate the anoxic conditions during the deposition the Palana shale sediments (Figure 14a). This interpretation is also corroborated by the association between the Ca, Mg and Al elements and their ratios of 100*Mg/Al and Ca/Mg (Lei et al., 2002; Zhang et al., 2020; Xu et al., 2022). In this case, a low 100*Mg/Al ratio of < 1 usually indicates freshwater conditions, while values 1 < 100*Mg/Al < 10 result in a brackish water and 100*Mg/Al ratio of >10 implies the salinity water deposition conditions (Lei et al., 2002; Zhang et al., 2020). In our case, the studied black shale facies of the Palana Formation exhibit 100*Mg/Al ratio between 1.32 and 2.5 (Table 2), indicating that this black shale facies was deposited in of the moderate salinity (brackish water) conditions of the water column during the Paleocene-Eocene period, as demonstrated by the relationship between sulfur content and relatively high values of the Ca/Mg ratio in the range of 1.8-3.88 (Figure 14b).

Preprints (www.preprints.org) | NOT PEER-REVIEWED | Posted: 24 November 2023 doi:10.20944/preprints202311.1550.v1

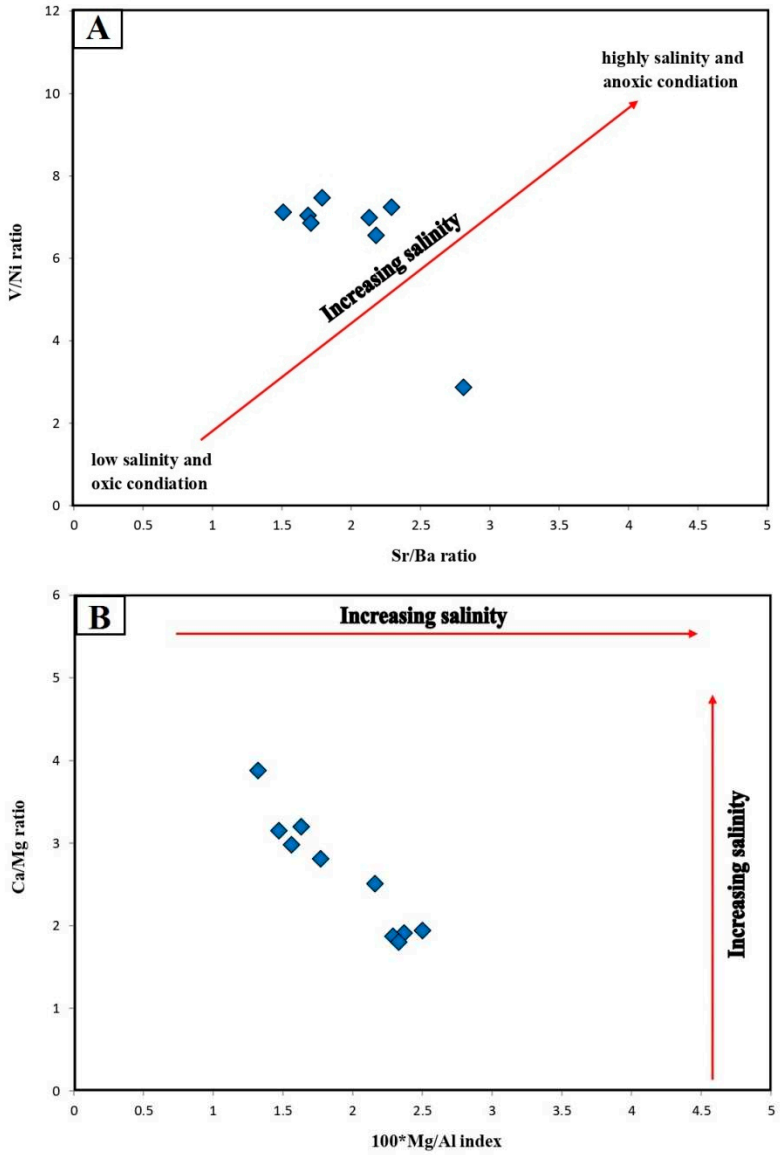

Figure 14. (A) Relationship between Sr/Ba and V/Ni ratios, and (B) Ca/Mg vs. 100*Mg/Al ratios plot, showing brackish water during deposition time (Paleocene-Eocene) in the studied black shale samples of the Palana Formation.

In addation, the upwelling processes affects the periodic influx of large masses of nutrients into the photic zone, whereas the bioproductivity is closely related to nutrient supply in the sea (Strakhov, 1960; Rostovtseva and Khan, 2017).

Currently, a number of inorganic geochemical elements such as Mo, Cd, Mn and Co elements have been used to indicate the impact the vertical circulation of sea water (upwelling systems) on the sedimentogenesis of black shales (Brumsack, 2006; Sweere et al., 2016; Zhang et al., 2018; Lu et al., 2019). In this case, upwelling zones show low abundances of both Co and Mn elements, while the contents of these elements Co and Mn are relatively high in restricted basins (Sweere et al., 2016). This may be attributed to an insufficient fluvial input supply in regions affected by upwelling systems (Sweere et al., 2016), where the Co and Mn enrichment in marine sediments is controlled by detrital input and authigenic enrichment (Lyons et al., 2003). However, the Co*Mn module has been developed to and show that values above 0.40 indicate the limitation of the marine basin and Co*Mn below 0.4 is typical for upwelling conditions.

Preprints (www.preprints.org) | NOT PEER-REVIEWED | Posted: 24 November 2023 doi:10.20944/preprints202311.1550.v1

In this study, high upwelling conditions during the Paleocene-Eocene time was recognized based on the high Co*Mn of smaller than 0.40 (0.004-0.22). This interpretation is corroborated by the association between the Co*Mn module and the Al2O3 content, as shown in Figure 15a. Similarly, the relatively higher Cd element together with an increase in organic matter of the studied black shales of the Palana Formation indicates upwelling processes in water bodies, with high primary bioproductivity during the deposition period (Conway and John, 2015). This finding clearly agrees with the directly proportional between the Cd and TOC contents (Figure 15b).

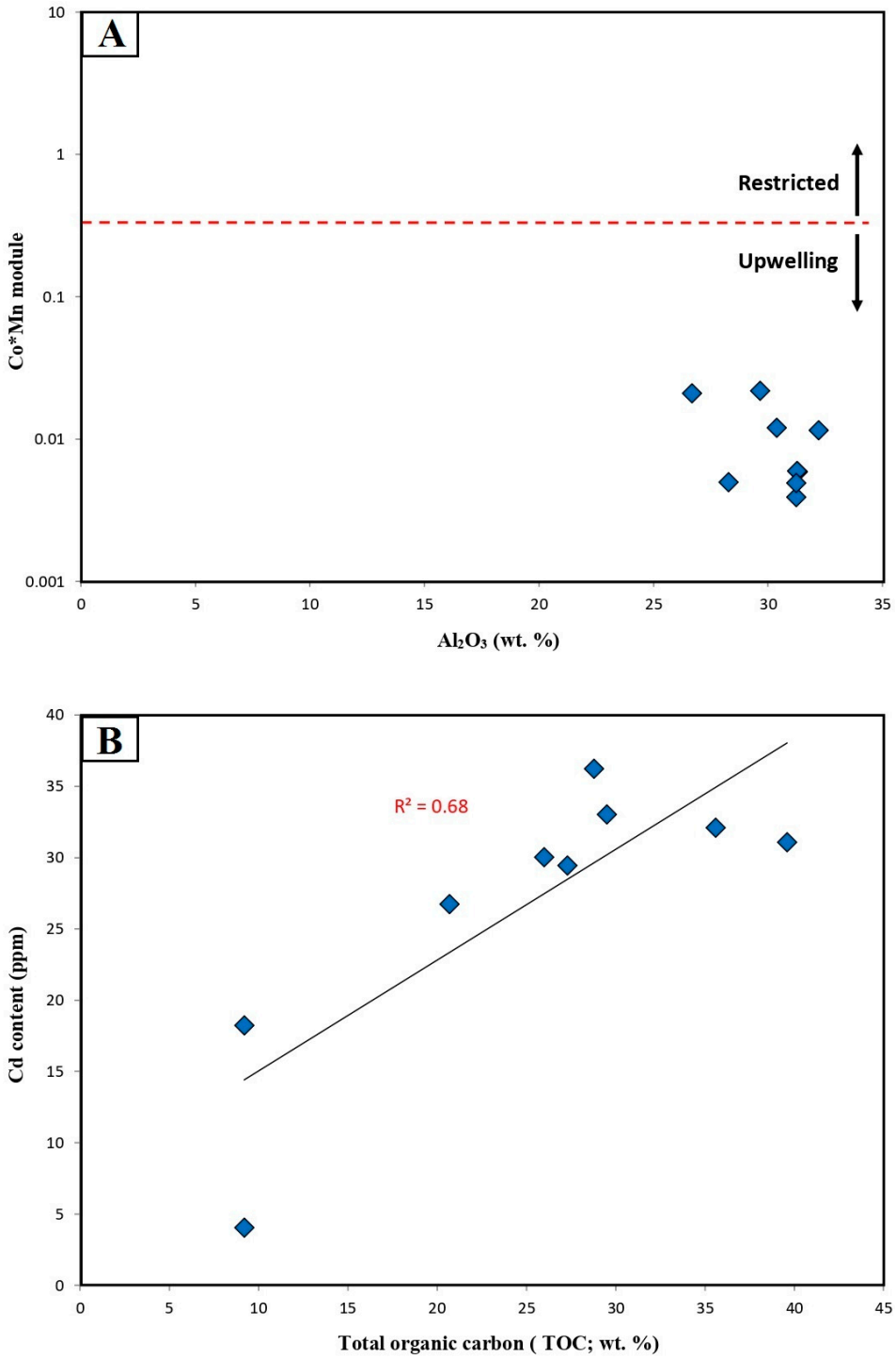

Figure 15. (A) cross-plot of the Co*Mn vs. Al2O3, showing upwelling activity during deposition time (Paleocene-Eocene) the studied black shale samples of the Palana Formation, and (B) Relationship between TOC and Cd contents, showing positive correlation.

 doi:10.20944/preprints202311.1550.v1

5.2. Paleoclimate Evolution during the Paleocene-Eocene

Paleoclimatic conditions have been suggested as one of the major factors controlling the biological productivity within the photic zone of the water columns, whereas the increased bioproductivity in the water is related to enhanced to humid-warm climate conditions (Jia et al., 2013; Adegoke et al., 2015; Hakimi et al., 2016).

In this study, the paleoclimate reconstruction during the Paleocene-Eocene was attempted based on a variety of climate indexes, including Sr/Cu, Rb/Sr, Ga/Rb and SiO2/Al2O3 ratios. These elements ratios are proposed and widely used to reconstruct the paleoclimate conditions (Lerman and Wang, 1989; Jia et al., 2013; Adegoke et al., 2015; Hakimi et al., 2016).

The Sr/Cu ratio is extensively to differentiate between a hot-arid (Sr/Cu > 10) and a warm-humid (1.3–5.0) climates (Lerman and Wang, 1989; Yandoka et al., 2015; Song et al., 2016; Xu et al., 2021). In our case, the results show that the Sr/Cu ratios for most of the studied Palana shales exhibit low Sr/Cu ratio of < 5 (0.76-1.35), suggesting that a warm and humid climates prevailed during the depositional period of the Palana black shale facies. This interpretation of the warm-humid climatic conditions is also consistent with the lower Rb/Sr values of less than 0.01, because the high Rb/Sr ratios of > 1 generally indicate cold and arid climates (Bai et al., 2015).

This finding of the warm-humid climatic conditions is clear supported by the cross-plot of Rb/Sr against Sr/Cu (Figure 16a).

Moreover, the major oxides-based observations, which involve SiO2, Al2O3, K2O, and Na2O elements (Table 2), can also be used to characterize warm and humid climates (Felix, 1977; Moradi et al., 2016; Hakimi et al., 2016). The Al2O3 and K2O major oxides and their associated trace elements gallium (Ga) and rubidium (Rb) are widely accepted to examine the paleoclimatic conditions during the depositional period of the Palana organic-rich shale sediments (Hakimi et al., 2016). The Ga is associated with Al2O3, whereas the Rb is associated with K2O (Hieronymus et al., 2001; Beckmann et al., 2005; Ratcliffe et al., 2004).

However, the Al2O3 is generally enriched in kaolinite clay mineral and are known to be associated with warm climate (Hieronymus et al., 2001; Beckmann et al., 2005), whilst K2O is associated with illite clay mineral and reflecting a dry and cold climatic conditions (Ratcliffe et al., 2004).

In this study, the studied black shale of the Palana Formation is enriched in Al2O3 compared to very low K2O, with high ratio of Al/K (Table 2). The high abundance of the Al2O3 is probably attributed to the enrichment of the kaolinite clay mineral of up to 27.3%, as clearly show from the XRD results (Table 1) together with the species identification (SPI) of the QEMSCAN results (Figure 7). The high abundant of kaolinite clay minerals within the studied samples is believed to interpret the warm and humid climates during the Paleocene-Eocene, as supported from the Ga/Rb versus K2O/Al2O3 binary diagram (Figure 16b), as reported by Roy and Roser (2013).

Preprints (www.preprints.org) | NOT PEER-REVIEWED | Posted: 24 November 2023 doi:10.20944/preprints202311.1550.v1

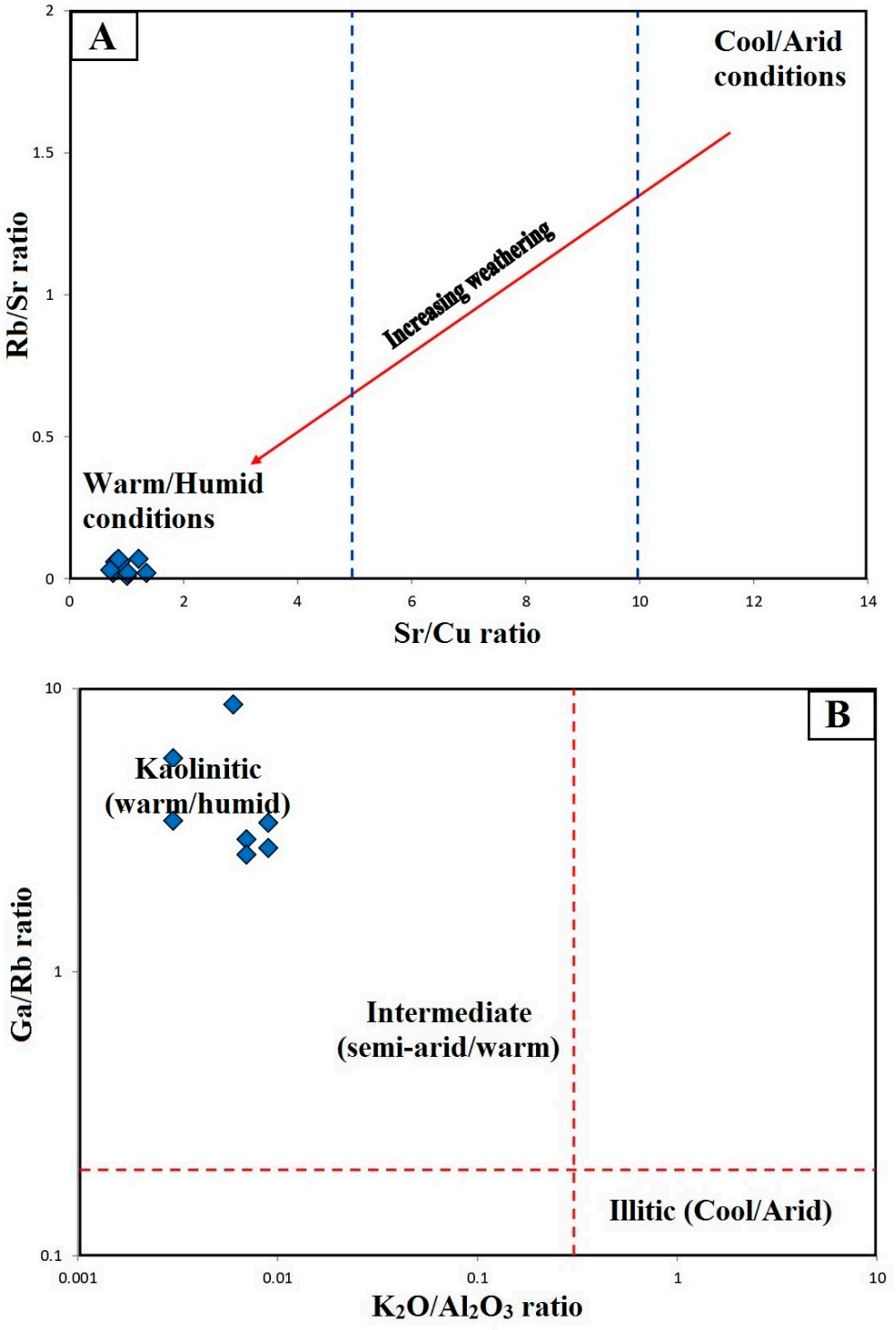

Figure 16. (Diagrams related to warm and humid climatic conditions during deposition time (Paleocene-Eocene) the studied black shale samples of the Palana Formation (A) Rb/Sr vs. Sr/Cu ratios plot and (B) Gr/Rb vs. K2O/Al2O3.

Moreover, the chemical weathering of the parent rock in the source area is generally affected by the climatic conditions (Moradi et al., 2016) and can be estimated using mineralogy and several geochemical indices of the major earth elements (Nesbitt and Young, 1982; Armstrong-Altrin et al. 2020). The chemical weathering intensity for sedimentary clastic rocks in the source area was also

Preprints (www.preprints.org) | NOT PEER-REVIEWED | Posted: 24 November 2023 doi:10.20944/preprints202311.1550.v1

widely evaluated using the mineralogical compositions together with several weathering indexes, including chemical index of alteration (CIA), plagioclase index of alteration (PIA). These CIA and PIA weathering indexes were calculated based on Al2O3, CaO, Na2O and K2O, as proposed by pervious published works (Nesbitt and Young, 1982; Harnois, 1988; Fedo et al., 1995) and used in recent workers such as Armstrong-Altrin et al. (2018), Ekoa Bessa et al. (2018), Mbale Ngama et al. (2019) and He et al. (2020). These authors reported that the CIA and PIA, with a value of 60 indicates low weathering, 60–75 moderate weathering and values of more than 75 indicate intensive weathering. Accordingly, the studied shale samples show high value of the CIA and PIA indexes between 93.45 and 96.00% (Table 2), indicating a high intensive degree of chemical weathering. This interpretation of the high chemical weathering trends is confirmed by the ternary diagram (A-CN-K) of Nesbitt and Young (1984), as shown in Figure 17. Based on the A-CN-K ternary diagram, most of the studied shale samples of the Palana Formation were plotted above the line of plagioclase and k-feldspar and clustered near the A-CN line towards the kaolinite composition, exhibiting a high degree of chemical weathering (Figure 18). This is in agreement with the high abundance of clay mineral, with high contributions of kaolinite and dickite clay minerals (Table 1), which are formed by the weathering of silicates (primarily feldspar) (Deer et al., 1975). Therefore, the original shale rocks of the Palana Formation were highly weathered in warm and humid climates during the Paleocene-Eocene period.

In addition, the warm water period during the deposition of the Palana shale samples (Paleocene-Eocene) also confirms from the high abundance of phytoplankton blooms (Figure 5), whereas the growth and decomposition of phytoplanktons are accelerated in warm water and decreased during the cold-water condition. In this way, the presence of high phytoplankton algae and other microorganisms in the analyzed Palana black shale sediments is probably due to the prevailing long warm-water episodes during the Paleocene-Eocene. However, the evidence for the presence of the richness of phytoplankton algae during the warm and humid climatic conditions is also demonstrated and supported from the occurrence of barite mineral associated with organic matter (Figure 8B), and relatively high-barium (Ba) trace element in the black shale intervals of the Palana Formation (Table 2), which are tightly connected with a high primary productivity (Ran et al., 2015; Wang et al., 2018; Zou et al., 2019), because the upwelling brings abundant nutrients to the surface seawater during the same time (Figure 15a).

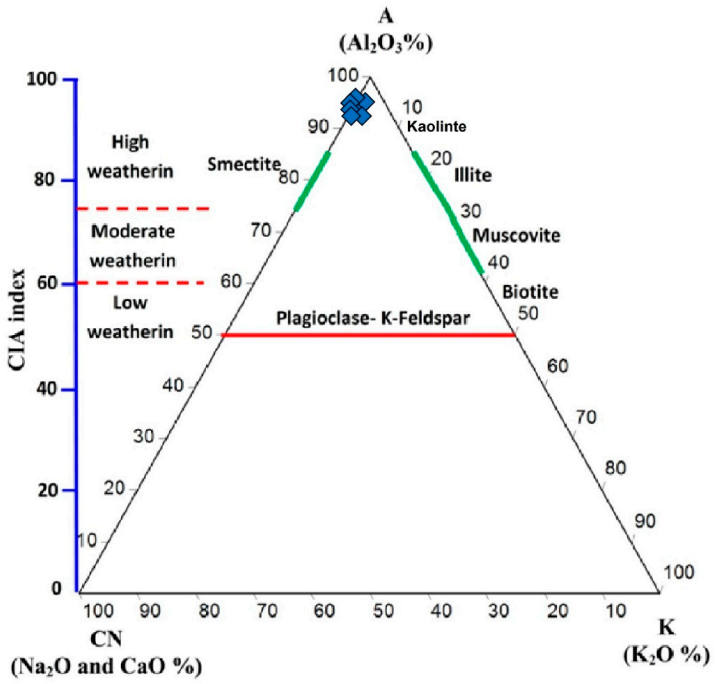

Figure 17. A-K-CN ternary diagram, showing high intensive degree of chemical weathering during deposition time (Paleocene-Eocene) the studied black shale samples of the Palana Formation.

Preprints (www.preprints.org) | NOT PEER-REVIEWED | Posted: 24 November 2023 doi:10.20944/preprints202311.1550.v1

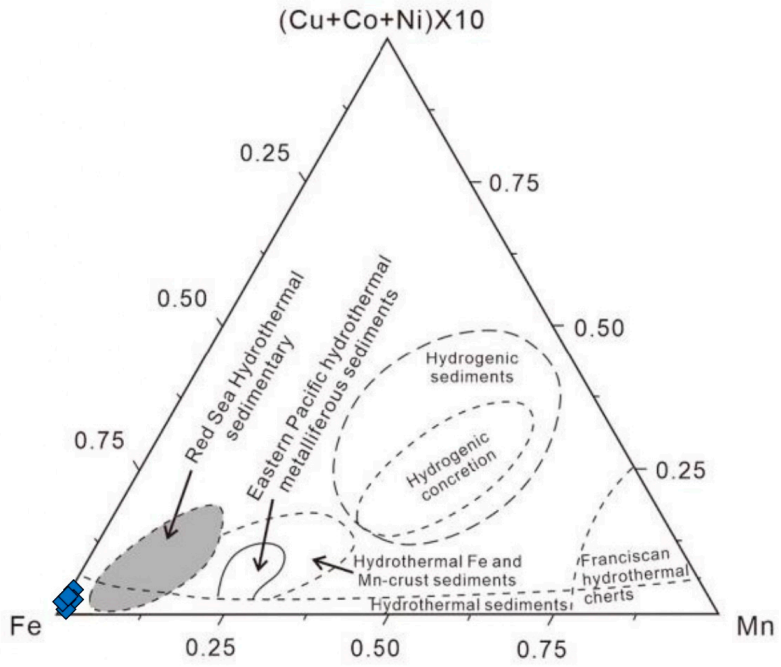

Figure 18. Fe-Mn-(Cu + Co + Ni) × 10 ternary diagram (Bostrom et al., 1973; Qi et al., 2004), showing high hydrothermal activity during deposition time (Paleocene-Eocene) in the studied black shale samples of the Palana Formation.

5.3. Hydrothermal and Volcanic Activity during the Paleocene-Eocene

The hydrothermal activity is commonly closely to the intrusion or eruption of magma and related to the strong rifting tectonic phase (Skinner, 1979; Qi et al., 2004; Zhang et al., 2019).

In the studied Bikaner-Nagaur Basin, most of the faults in the basin were resulted by initial phase of rifting as a result of the Pan-African orogeny during Late Proterozoic (Pollastro et al. 1999; Al-Husseini 2000; Dmitry et al. 2007). However, this fault system of the basin witnessed multiple phases of reactivation as a result of younger tectonic episodes such as extension during Permo-Triassic, early-to-mid Jurassic and compression during Tertiary time (Manda et al., 2022). These fault systems of the Paleozoic and Mesozoic period provided migration pathways potential for the rise of deep hydrothermal fluids.

In order to estimate the hydrothermal activities during the Paleocene-Eocene, this study used the hydrothermal geochemical indicators and discrimination diagram of major and trace elements. However, the Fe and Mn elements can be employed to ascertain the influence of hydrothermal activity on sedimentary rocks, which are mostly easily and active enriched in sediments during hydrothermal activities (Adachi et al., 1986). The Fe and Mn major elements were integrated together with the Ti element and used to calculate the (Fe + Mn)/Ti ratio, which is a good indicator to evaluate the hydrothermal activities and their impact on the sedimentary rocks (Strakhov, 1976; Adachi et al., 1986). (Fe + Mn)/Ti ratio of < 15 indicates strong hydrothermal indication, while (Fe + Mn)/Ti ratio of >15 indicates influence of week hydrothermal activities deposition under oxic conditions (Qi et al., 2004; Wang et al., 2017). In this case, the studied black shale samples of the Palana Formation exhibit (Fe + Mn)/Ti ratio between 8.61 and 22.87, with an average value of 14.75 (Table 2), indicating generally strong hydrothermal activities during the Paleocene-Eocene period. This interpretation of the strong hydrothermal activities is confirmed by the relationship between the Fe and Mn elements and the sum of the Cu, Co, and Ni trace elements (Bostrom et al., 1973; Qi et al., 2004). The richness of the Fe element than Mn, Cu, Co, and Ni trace elements of all examined samples (Table 2), supports the inference of strong hydrothermal activities during the Paleocene-Eocene period, which is closed and quite similar to the Red sea hydrothermal sedimentary based on the Fe-Mn-(Cu + Co + Ni) × 10

 doi:10.20944/preprints202311.1550.v1

ternary diagram of Bostrom et al. (1973) and Qi et al. (2004), as shown in Figure 18. Moreover, the high concentrations of olivine together with significant amounts of other silica minerals i.e., quartz, apophyllite and tridymite in these black shale intervals (Table 1) are mostly considered to be of volcanic origin and supports hydrothermal activities during the Paleocene-Eocene period. These volcanic activities during the Paleocene-Eocene period in this case are considered influx of large masses of ash accumulations during the volcanic eruption. The relatively high contents of zeolite mineral (up to 6.1%) in the Palana shale facies is indicative of increased volcanic-ash. However, the high amounts of volcanic ash into aqueous environments may lead to the dissolution of absorbed sediments, including metal salts, mainly supplying a high concentration of the nutrients for organisms, thereby enhancing and increasing the primary bioproductivity (Langmann et al., 2010; Duggen et al., 2010). In this case, the most of the nutrients are phosphorus (P) and nitrogen (N), which commonly occurs in sea-water.

In term of nutrient P content, the studied Palana shale samples are enriched in P, with a P_2O_3 range of 0.14-0.50% together with high Fe contents (Table 2), indicating that nutrients were transported and concentrated in the these shales after deposition and hydrolyzation of volcanic-ash (Chen et al., 2021). This interpretation is confirmed by the obvious positive correlation between P_2O_3 and zeolite-derived volcanic (Figure 19a). In addition, the significantly positive correlation between P_2O_3 and Sr/Ba ratio (R^2= 0.56; Figure 19b) also indicates that the primary productivity of the aquatic organisms was due to input of volcanic ash containing abundant nutrient salts (Chen et al., 2021).

Preprints (www.preprints.org) | NOT PEER-REVIEWED | Posted: 24 November 2023 doi:10.20944/preprints202311.1550.v1

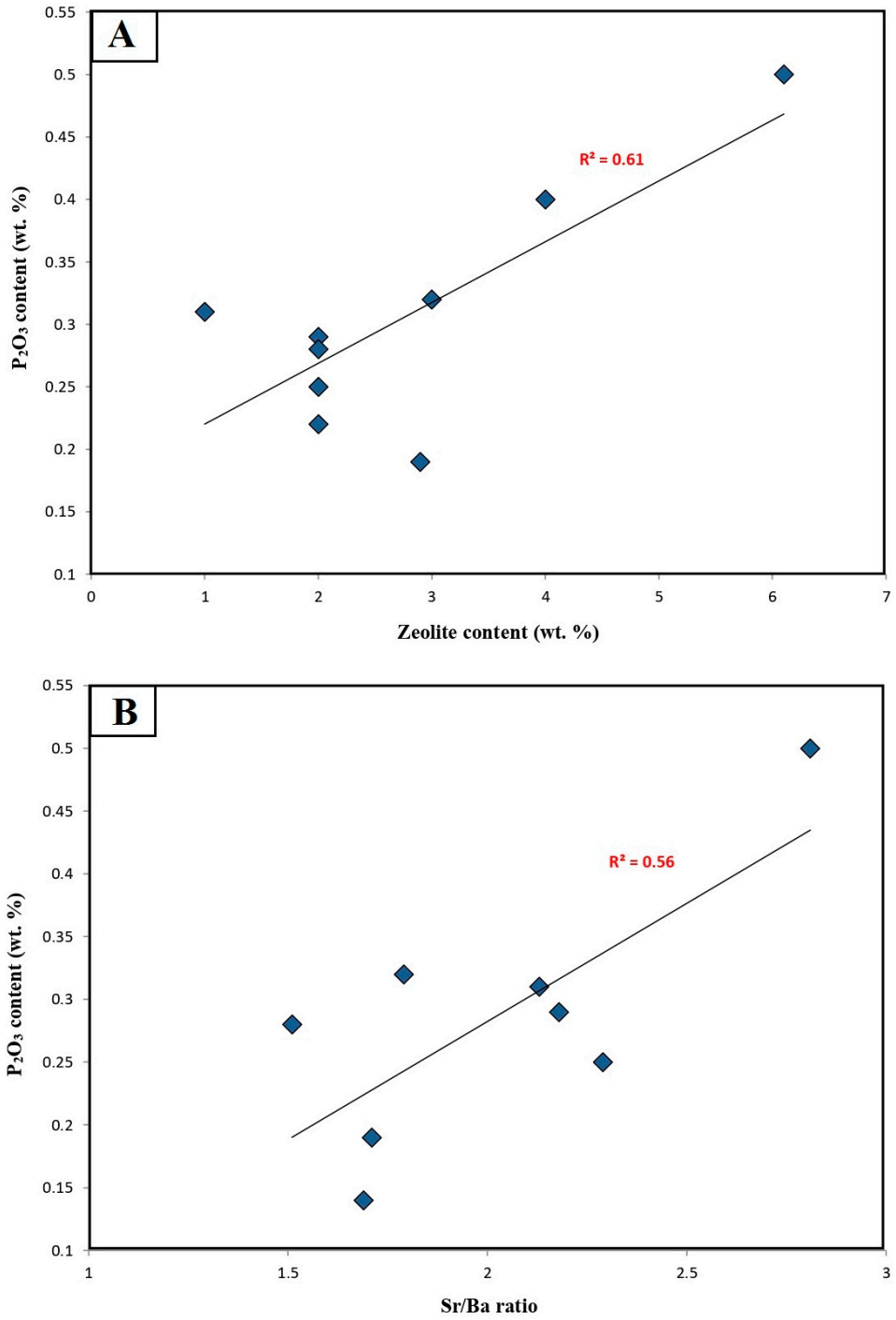

Figure 19. Plots of (A) P2O3 content versus zeolite mineral content, and (B) P2O3 content versus Sr/Ba ratio of the studied black shale samples of the Palana Formation, showing a good positive correlations, with R2= 0.61 and R2= 0.56, respectively.

6. Conclusions

Organic-rich shale facies of the Palana Formation from a Gurha mine in western Rajasthan, India were investigated based on organic geochemistry, mineralogical and elemental composition together with microscopic examinations to evaluate the main sedimentary paleoenvironmental factors and volcanic activity during the Paleocene-Eocene influencing the high organic carbon accumulation. Based on the results, we conclude the following:

- The black shale facies of the Paleocene-Eocene Palana Formation exhibit rich TOC and S contents of up to 36.23 wt. % and 2.24 wt. %, respectively, revealing normal marine setting and anoxic environmental conditions.
- The Palana shales are clay-rich lithofacies, ranging from siliceous mudstone to silica-rich argillaceous mudstone, with high abundance of clay and silica minerals, as indicated by XRD data together with species identification (SPI) and SEM of the QEMSCAN results.
- Microscopic examinations reveal that the OM in the Palana clay-rich facies was primarily derived from algae and other bacterial organism, along with foraminifer assemblages, which favored marine anoxic environmental conditions.
- Different redox-sensitive trace elements along with their ratios of the clay-rich shale facies of the Palana Formation indicate anoxic environmental conditions were recognized during the Paleocene-Eocene period.
- The mineralogical and elemental compositions show warm and humid climates, with an intensive degree of chemical weathering took place during the deposition of the Paleocene-Eocene Palana clay-rich facies.
- The results highlighted in this study suggest that the high organic carbon accumulation in the black shale facies of the Palana Formation was mainly controlled by the sedimentary factors i.e., high bioproductivity and preservation of organic matter together with volcanic activities during the Paleocene-Eocene period

Acknowledgments: The authors thank Director RGIPT for allowing them to conduct this research and provide the facilities. The second author acknowledges the University Malaya postdoctoral fellowship scheme associated with grant number IF064-2019. The authors extend their sincere appreciation to the Researchers Supporting Project number (RSP2023R92) at King Saud University in Riyadh, Saudi Arabia. This work was also supported by the Ministry of Science and Higher Education of the Russian Federation under agreement No. 075-15-2022-299.

Conflicts of Interest: The authors declare that the research was conducted in the absence of any commercial or financial relationships that could be construed as a potential conflict of interest.

References

1. Adachi, M., Yamamoto, K., Sugisaki, R., 1986. Hydrothermal chert and associated siliceous rocks from the northern Pacific their geological significance as indication of ocean ridge activity. Sediment. Geol. 47, 125–148.
2. Adegoke, A.K., Abdullah, W.H., Hakimi, M.H., Sarki Yandoka, B.M., 2014. Geochemical characterisation of Fika Formation in the Chad (Bornu) Basin, northeastern Nigeria: implications for depositional environment and tectonic setting. Appl. Geochem. 43, 1–12.
3. Ahmed, A., Jahandad, S., Hakimi, M. H., Gharib, A. F., Mehmood, S., Kahal, A. Y., & Lashin, A. (2022). Organic matter characteristics and conventional oil potentials of shales from the Early Jurassic Datta Formation in the Upper Indus Basin, Northern Pakistan. Journal of Asian Earth Sciences, 224, 104975.
4. Algeo, T.J., Liu, J.S., 2020. A re-assessment of elemental proxies for paleoredox analysis. Chem. Geol. 540, 119549.
5. Algeo, T.J., Maynard, J.B., 2004. Trace-element behavior and redox facies in core shales of Upper Pennsylvanian Kansas-type cyclothems. Chem. Geol. 206, 289–318.
6. Al-Husseini, M.I., 2000. Origin of the Arabian plate structures: Amar collision and Najd Rift. Geo Arabia 5:527–542.
7. Alqubalee, A.M., Babalola, L.O., Abdullatif, O.M., Eltom, H.A., 2021. Geochemical Characterization of Subsurface Upper Ordovician Glaciogenic Deposits: Implications for Provenance, Tectonic Setting, and Depositional Environments. Arab. J. Sci. Eng. 1–19.
8. Amao, A.O., Al-Otaibi, B., Al-Ramadan, K., 2022. High-resolution X–ray diffraction datasets: Carbonates. Data Br. 42,
9. Armstrong-Altrin, J.S., Ramos-Vázquez, M.A., Hermenegildo-Ruiz, N.Y., Madhavaraju, J., 2020. Microtexture and U–Pb geochronology of detrital zircon grains in the Chachalacas beach, Veracruz State, Gulf of Mexico. Geological J.

10. Ayling, B., Rose, P., Petty, S., Zemach, E., Drakos, P., 2012. QEMSCAN® (Quantitative Evaluation of Minerals by Scanning Electron Microscopy): capability and application to fracture characterization in geothermal systems. Geotherm. Reserv. Eng. Work. 11.
11. Bai, Y.Y., Liu, Z.J., Sun, P.C., Liu, R., Hu, X.F., Zhao, H.Q., Xu, Y.B., 2015. Rare earth and major element geochemistry of Eocene fine-grained sediments in oil shale and coal-bearing layers of the Meihe Basin, Northeast China. J. Asian Earth Sci. 97, 89–101.
12. Bechtel, A., Gratzer, R., Sachsenhofer, R.F., 2001. Chemical characteristics of upper cretaceous (Turonian) jet of the gosau group of gams/hieflau (styria, Austria). Int. J. Coal Geol. 46, 27-49.
13. Bechtel, A., Jia, J.L., Strobl, S.A.I., Sachsenhofer, R.F., Liu, Z.J., Gratzer, R., Püttmann, W., 2012. Paleoenvironmental conditions during deposition of the Upper Cretaceous oil shale sequences in the Songliao Basin (NE China): implications from geochemical analyses. Organic Geochemistry 46, 76–95.
14. Beckmann, B., Flogel, S., Hofmann, P., Schulz, M., Wagner, T., 2005. Orbital forcing of Cretaceous river discharge in tropical Africa and ocean response. Nature 437, 241-244.
15. Berner, R.A., Raiswell, R., 1983. Burial of organic carbon and pyrite sulfur in sediments over Phanerozoic time: a new theory. Geochim. Cosmochim. Acta 47, 855-862.
16. Bordenave, M. L., Espitalié, J., Leplat, P. O. J. L., Oudin, J. L., & Vandenbroucke, M. (1993). Screening techniques for source rock evaluation. Applied petroleum geochemistry, 217-278.
17. Boström, K., Kraemer, T., Gartner, S., 1973. Provenance and accumulation rates of opaline silica, Al, Ti, Fe, Mn, Cu, Ni and Co in Pacific pelagic sediments. Chem. Geol. 11 (2), 123–148.
18. Brumsack, H.J., 2006. The trace metal content of recent organic carbon-rich sediments: implications for Cretaceous black shale formation. Palaeogeogr. Palaeoclimatol. Palaeoecol. 232 (2–4), 344–361.
19. Calvert S.E., Pedersen T.F., 2007. Chapter fourteen elemental proxies for palaeoclimatic and palaeoceanographic variability in marine sediments: interpretation and application. Developments in marine geology. 1, 567–644.
20. Carroll, A.R, Bohacs, K.M., 1999. Stratigraphic classification of ancient lakes: balancing tectonic and climatic controls. Geology 27, 99–102.
21. Chen, X., Zhang, B., Huang, H., Mao, Z., 2021. Controls on Organic Matter Accumulation of the Triassic Yanchang Formation Lacustrine Shales in the Ordos Basin, North China. ACS Omega 6, 26048−26064
22. Conway, T. M., John S.G., 2015. Biogeochemical cycling of cadmium isotopes along a highresolution section through the North Atlantic Ocean. Geochim. Cosmochim. Acta. 148, 269283.
23. Dashtgard, Sh.E., Wang, A., Pospelova, V., Wang, P.-L., La Croix, A., Ayranci, K., 2022. Salinity indicators in sediment through the fluvial-to-marine transition (Fraser River, Canada). Sci. Rep. 12, 14303
24. Deng, H.W., Qian, K., 1993. Analysis on Sedimentary Geochemistry and Environment. Science Technology Press, Gansu, pp. 15–85 (in Chinese).
25. Dmitry A, Al-Husseini MI, Yumiko I (2007) Review of middle east paleozoic plate tectonics. Geo Arabia 12:5–56.
26. Duggen, S., Olgun, N., Croot, P., Hoffmann, L., Dietze, H., Delmelle, P., Teschner, C., 2010. The role of airborne volcanic ash for the surface ocean biogeochemical iron-cycle: A review. Biogeosciences 7, 827−844.
27. Fedo, C.M., Nesbitt, H.W., Young, G.M., 1995. Unraveling the effects of potassium metasomatism in sedimentary rocks and paleosols, with implications for paleoweathering conditions and provenance. Geology 23, 921–924.
28. Felix, N.S., 1977. Physico-Chemical Studies on Bentonites with Special Reference to Fayoum Deposits (Ph.D. Thesis). Fac. of Sci., Cairo, Univ, Egypt.
29. Galarraga, F., Reategui, K., Martïnez, A., Martínez, M., Llamas, J.F., Marquez, G., 2008. V/Ni ratio as a parameter in palaeoenvironmental characterisation of nonmature medium-crude oils from several Latin American basins. J. Pet. Sci. Eng. 61, 9-14.
30. Hatch, J.R., Leventhal, J.S., 1992. Relationship between inferred redox potential of the depositional environment and geochemistry of the upper pennsylvanian (missourian) Stark shale member of the dennis limestone, wabaunsee county, Kansas, USA. Chem. Geol. 99, 65–82.
31. Hakimi, M.H., Wan, H.A., Shalaby, M.R., 2011. Organic geochemical characteristics and depositional environments of the Jurassic shales in the Masila Basin of Eastern Yemen. GeoArabia 16, 47-64.
32. Hakimi, M.H., Wan Hasiah, A., Shalaby, M.R., 2012. Molecular composition and organic petrographic characterization of Madbi source rocks from the Kharir Oilfield of the Masila Basin (Yemen): palaeoenvironmental and maturity interpretation. Arab. J. Geosci. 5, 817-831.

33. Hakimi, M.H., Wan Hasiah, A., 2013. Organic geochemical characteristics and oil generating potential of the Upper Jurassic Safer shale sediments in the Marib-Shabowah Basin, western Yemen. Organic Geochemistry 54, 115–124.
34. Hakimi, M.H., Abdullah, W.H., Alqudah, M., Makeen, Y.M., Mustapha, K.A., 2016. Reducing marine and warm climate conditions during the Late Cretaceous, and their influence on organic matter enrichment in the oil shale deposits of North Jordan. Int. J. Coal Geol. 165, 173-189.
35. Hatem, BA. Abdullah, WH., Hakimi, MH., Mustapha, KA (2016). Origin of organic matter and paleoenvironment conditions of the Late Jurassic organic-rich shales from Shabwah sub-basin (western Yemen): Constraints from petrology and biological markers. Marine and Petroleum Geology 72 (2016) 83-97
36. He, T.H., Lu, S.F., Li, W.H., Sun, D.Q., Pan, W.Q., Zhang, B.S., Tan, Z.Z., Ying, J.F., 2020. Paleoweathering, hydrothermal activity and organic matter enrichment during the formation of earliest Cambrian black strata in the Northwest Tarim Basin, China. J. Pet. Sci. Eng. 189 https://doi.org/10.1016/j.petrol.2020.106987.
37. Hieronymus, B., Kotschoubey, B., Boulegue, J., 2001. Gallium behavior in some contrasting lateritic profiles from Cameroon and Brazil. J. Geochem. Explor 72, 147-163.
38. Jarvie, D. M., Hill, R. J., Ruble, T. E., & Pollastro, R. M., 2007. Unconventional shale-gas systems: The Mississippian Barnett Shale of north-central Texas as one model for thermogenic shale-gas assessment. AAPG bulletin, 91(4), 475-499.
39. Jia, J., Bechtel, A., Liu, Z., Susanne, A.I., Strobl, P.S., Reinhard, F.S., 2013. Oil shale formation in the upper cretaceous nenjiang formation of the songliao basin (NE China): implications from organic and inorganic geochemical analyses. Int. J. Coal Geol. 113, 11-26.
40. Jones, B., Manning, D.A., 1994. Comparison of geochemical indices used for the interpretation of palaeoredox conditions in ancient mudstones. Chem. Geol. 111, 111–129.
41. Katz, B.J., 2005. Controlling factors on source rock developmentda review of productivity, preservation and sedimentation rate. In: Harris, N.B. (Ed.), The Deposition of Organic-carbon-rich Sediments: Models, Mechanisms, and Consequences, vol. 82. SEPM Special Publication, pp. 7-16.
42. Kumar, A., 2022. Tertiary Coal and Lignite Deposits of India and their Source Rock Potential: A Review on the Contribution of the Indian Coal Petrologists. Journal of the Geological Society of India, 98(12), 1745-1753.
43. Kumar, A., Singh, A. K., Paul, D., & Kumar, A. (2020). Evaluation of hydrocarbon potential with insight into climate and environment present during deposition of the Sonari lignite, Barmer Basin Rajasthan. Energy and Climate Change, 1, 100006.
44. Kumar, A., Hakimi, M. H., Singh, A. K., Abdullah, W. H., Zainal Abidin, N. S., Rahim, A., Mustapha, K.A., & Yelwa, N. A. (2022). Geochemical and Petrological Characterization of the Early Eocene Carbonaceous Shales: Implications for Oil and Gas Exploration in the Barmer Basin, Northwest India. ACS omega, 7(47), 42960-42974.
45. Langmann, B., Zaksek, K., Hort, M., Duggen, S., 2010. Volcanic ash as fertilizer for the surface ocean. Atmos. Chem. Phys. 10, 38913899.
46. Lei, B., Que, H.P., Hu, N., Niu, Z.J., Wang, H., 2002. Geochemistry and sedimentary environments of the Palaeozoic siliceous rocks in western Hubei. Sediment. Geol. Tethyan Geol. 22, 70–79 (in Chinese with English abstract).
47. Li, T.Y., He, S., Yang, Z., 2008. The marine source rock formation conditions and control factors. Geological Science and Technology Information 27, 63–70 (in Chinese with English abstract).
48. Lu, Y., Jiang, S., Lu, Y., Xu, S., Shu, Y., Wang, Y., 2019. Productivity or preservation? The factors controlling the organic matter accumulation in the late Katian through Hirnantian Wufeng organic-rich shale, South China. Mar. Petrol. Geol. 109, 22–35.
49. Lyons, T.W., Werne, J.P., Hollander, D.J., Murray, R.W., 2003. Contrasting sulfur geochemistry and Fe/Al and Mo/Al ratios across the last oxic-to-anoxic transition in the Cariaco Basin, Venezuela. Chem. Geol. 195, 131–157.
50. Makeen, Y.M., Hakimi, M.H., Abdullah, W.H., 2015. The origin, type and preservation of organic matter of the Barremian-Aptian organic-rich shales in the Muglad Basin, Southern Sudan, and their relation to paleoenvironmental and paleoclimate conditions. Mar. Pet. Geol. 65, 187-197.
51. Mathews, R. P., Singh, B. D., Singh, V. P., Singh, A., Singh, H., Shivanna, M., ... & Chetia, R. (2020). Organo-petrographic and geochemical characteristics of Gurha lignite deposits, Rajasthan, India: Insights into the

palaeovegetation, palaeoenvironment and hydrocarbon source rock potential. Geoscience Frontiers, 11(3), 965-988.

52. Mohialdeen, I.M.J., Hakimi, M.H., Al-Beyati, F.M., 2013. Geochemical and petrographic characterization of late Jurassic-early cretaceous Chia Gara formation in northern Iraq: palaeoenvironment and oil-generation potential. Mar. Petrol. Geol. 43, 166-177.
53. Moradi, A.V., Sarı, A., Akkaya, P., 2016. Geochemistry of the Miocene oil shale (hançili formation) in the Çankırı-Çorum basin, Central Turkey: implications for paleoclimate conditions, source–area weathering, provenance and tectonic setting. Sediment. Geol. 341, 289–303.
54. Mukherjee, M., & Misra, S. (2018). A review of experimental research on Enhanced Coal Bed Methane (ECBM) recovery via CO2 sequestration. Earth-Science Reviews, 179, 392-410.
55. Nesbitt, H.W., Young, G.M., 1982. Early Proterozoic climates and plate motions inferred from major element chemistry of lutites. Nature 299, 715–717.
56. Omar, N., McCann, T., Al-Juboury, A.I., Franz, S.O., 2020. Petrography and geochemistry of the Middle-Upper Jurassic Banik section, northernmost Iraq—implications for paleoredox, evaporitic and diagenetic conditions. N. Jb. Geol. Paleont. Abh. 297, 125–152.
57. Orhan, H., Delikan, A., Demir, A., Kapan, S., Olgun, K., Ozmen, A., Sayin, Ü., Ekici, G., Aydin, H., Nazik, A., 2019. Geochemical evidences of paleoenvironmental changes in late quaternary lacustrine sediments of the konya closed basin (konya, Turkey). In: Zhang, Z., Khelifi, N., Mezghani, A., Heggy, E. (Eds.), Patterns and Mechanisms of Climate, Paleoclimate and Paleoenvironmental Changes from Low Latitude Regions. Springer Berlin, Germany, pp. 73–76.
58. Pollastro, R.M., 1999. Ghaba Salt Basin province and Fahud Salt Basin province—Oman: geological overview and total petroleum systems. United States Geol Sur Bull 2167:1–41.
59. Price, G.D., 1999. The evidence and implications of polar-ice during the Mesozoic. Earth Sci. Rev. 48, 183–210.
60. Qi, H.W., Hu, R.Z., Su, W.C., Qi, L., Feng, J.Y., 2004. Continental hydrothermal sedimentary siliceous rock and genesis of superlarge germanium (Ge) deposit hosted in coal: a study from the Lincang Ge deposit, Yunnan, China. Sci. China Ser. D Earth Sci. 47, 973–984.
61. Qian, G., Li, Y., Gerson, A.R., 2015. Applications of surface analytical techniques in Earth Sciences. Surf. Sci. Rep. 70, 86–133. https://doi.org/10.1016/j.surfrep.2015.02.001
62. Ran, B., Liu, S., Jansa, L., Sun, W., Yang, D., Ye, Y., Wang, S., Luo, C., Zhang, X., Zhang, C., 2015. Origin of the Upper Ordovician–lower Silurian cherts of the Yangtze block, South China, and their palaeogeographic significance. J. Asian Earth Sci. 108, 1–17.
63. Ratcliffe, K.T., Wright, A.M., Hallsworth, C., Morton, A., Zaitlin, B.A., Potocki, D., Wray, D.S., 2004. Alternative correlation techniques in the petroleum industry: an example from the (lower cretaceous) basal quartz, southern Alberta. Bullet. Am. Assoc. Pet. Geol. 88, 419-432.
64. Read, J.F., Kerans, C., Weber, L.J., Sarg, H.F., Wright, F.M., 1995. Milankovitch sea-level changes, cycles and reservoirs on carbonate platforms in green-house and ice-house worlds. SEPM Short. Course 35, 1–81.
65. Remírez, M.N., Algeo, T.J., 2020. Paleosalinity determination in ancient epicontinental seas: a case study of the T-OAE in the Cleveland Basin (UK). Earth Sci. Rev. 201, 103072.
66. Roy, A. B., Jakhar, S. R., 2002. Geology of Rajasthan (Northwest India) precambrian to recent. Scientific Publishers.
67. Schopf, J. M., 1960. Field description and sampling of coal beds (p. 67). Washington, DC: US Government Printing Office.
68. Schwarzkopf, T.A., 1993. Model for prediction of organic carbon in possible source rocks. Maine Pet. Geol. 10, 478-492.
69. Singh, P. K., Rajak, P. K., Singh, V. K., Singh, M. P., Naik, A. S., & Raju, S. V. (2016). Studies on thermal maturity and hydrocarbon potential of lignites of Bikaner–Nagaur basin, Rajasthan. Energy Exploration & Exploitation, 34(1), 140-157.
70. Singh, A., Shivanna, M., Mathews, R. P., Singh, B. D., Singh, H., Singh, V. P., Dutta, S., 2017. Paleoenvironment of Eocene lignite bearing succession from Bikaner-Nagaur Basin, western India: organic petrography, palynology, palynofacies and geochemistry. International Journal of Coal Geology, 181, 87-102.

71. Singh, A. K., Kumar, A., Hakimi, M. H., 2018. Organic geochemical and petrographical characteristics of the Nagaur lignites, Western Rajasthan, India and their relevance to liquid hydrocarbon generation. Arabian Journal of Geosciences, 11, 1-15.
72. Singh, A. K., Hakimi, M. H., Kumar, A., Ahmed, A., Abidin, N. S. Z., Kinawy, M., Mahdy, O.E., Lashin, A., 2020. Geochemical and organic petrographic characteristics of high bituminous shales from Gurha mine in Rajasthan, NW India. Scientific reports, 10(1), 1-19.
73. Singh, V. P., Singh, B. D., Mathews, R. P., Singh, A., Mendhe, V. A., Mishra, S., & Banerjee, M., 2022. Paleodepositional and Hydrocarbon Source-Rock Characteristics of the Sonari Succession (Paleocene), Barmer Basin, NW India: Implications from Petrography and Geochemistry. Natural Resources Research, 31(5), 2943-2971.
74. Shu, T., Dazhen, T., Hao, X., Jianlong, L., Xuefeng, S., 2013. Organic geochemistry and elements distribution in Dahuangshan oil shale, southern Junggar Basin: origin of organic matter and depositional environment. Int. J. Coal Geol. 115, 41-51.
75. Shukla, A., Jasper, A., Uhl, D., Mathews, R. P., Singh, V. P., Chandra, K., Chetia, R., Shukla, S., & Mehrotra, R. C., 2023. Paleo-wildfire signatures revealing co-occurrence of angiosperm-gymnosperm in the early Paleogene: Evidences from woody charcoal and biomarker analysis from the Gurha lignite mine, Rajasthan, India. International Journal of Coal Geology, 265, 104164.
76. Skinner, B., 1979. The many origins of hydrothermal mineral deposits. In: Barnes, H.L. (Ed.), Geochemistry of Hydrothermal Ore Deposits, second ed. John Wiley & Sons, New York, pp. 3–21.
77. Song, Y., Liu, Z., Meng, Q., Xu, J., Sun, P., Cheng, L., Zheng, G., 2016. Multiple controlling factors of the enrichment of organic matter in the upper cretaceous oil shale sequences of the Songliao basin, NE China: implications from geochemical analyses. Oil Shale 33, 142–166.
78. Strakhov N.M., 1960. Fundamentals of the theory of lithogenesis. M. Publishing House of the Academy of Sciences of the USSR.
79. Strakhov N.M., 1976. Problems of geochemistry of modern oceanic lithogenesis. M., Science.
80. Sweere, T., van den Boorn, S., Dickson, A. J, Reichart, G.-J., 2016. Definition of new trace-metal proxies for the controls on organic matter enrichment in marine sediments based on Mn, Co, Mo and Cd concentrations. Chem. Geol. 441, 235-245.
81. Talbot, M.R., 1988. The Origins of Lacustrine Oil Source Rocks: Evidence from the Lakes of Tropical African Geological Society London, vol. 40, pp. 29-43. Special Publication.
82. Tissot, P., & Welte, D. H. (1984). Petroleum formation and occurrence. Springer-verlag.
83. Tribovillard, N., Algeo, T.J., Lyons, T., Riboulleau, A., 2006. Trace metals as paleoredox and paleoproductivity proxies: an update. Chem. Geol. 232, 12–32.
84. Vincent, B., Rambeau, C., Emmanuel, L., Loreaue, J.P., 2006. Sedimentology and trace element geochemistry of shallow-marine carbonates: an approach to paleoenvironmental analysis along the Pagny-sur-Meuse section (Upper Jurassic, France). Facies 52, 69–84.
85. Wang, Z., Fu, X., Feng, X., Song, C., Wang, D., Chen, W., Zeng, S., 2017. Geochemical features of the black shales from the Wuyu Basin, southern Tibet: implications for paleoenvironment and paleoclimate. Geol. J. 52, 282297.
86. Wang, Y., Chen, B., Li, X., Wang, H., Chang, L., Jiang, S., 2018. Sedimentary characteristics of up-welling facies shale in lower Silurian Longmaxi Formation, northeast sichuan area. Acta. Petrol. Ei. Sinica. 39, 1092–1102.
87. Xie, H., Zhou, D., Li, Y., Pang, X., Li, P., Chen, G., Li, F., Cao, J., 2014. Cenozoic tectonic subsidence in Deepwater sags in the Pearl River Mouth Basin, northern South China Sea. Tectonophysics 615.
88. Xu, J., Liu, Z., Bechtel, A., Meng, Q., Sun, P., Jia, J., Cheng, L., Song, Y., 2015. Basin evolution and oil shale deposition during Upper cretaceous in the songliao basin (NE China): implications from sequence stratigraphy and geochemistry. Int. J. Coal Geol. 149, 9–23.
89. Xu, C., Shan, X.L., He, W.T., 2021a. The fluctuation of warm paleoclimatic controls on lacustrine carbonate deposition in the Late Cretaceous (late Santonian), Southern Songliao Basin, Northeast China. Int. J. Earth Sci. 111 https://doi.org/10.1007/ s00531-021-97402100-1.
90. Yandoka, B.M.S., Abdullah, W.H., Abubakar, M.B., Hakimi, M.H., Adegoke, A.K., 2015. Geochemical characterization of early Cretaceous lacustrine sediments of Bima Formation, Yola Sub-basin, northern Benue trough, NE Nigeria: organic matter input, preservation, paleoenvironment and paleoclimatic conditions. Mar. Petrol. Geol. 61, 82–94.

91. Zhang, B., Yao, S., Wignall, P.B., Hu, W., Ding, H., Liu, B., Ren, Y., 2018. Widespread coastal upwelling along the eastern paleo-tethys margin (south China) during the middle Permian (Guadalupian): implications for organic matter accumulation. Mar. Petrol. Geol. 97, 113–126.
92. Zhang, K., Song, Y., Jiang, S., Jiang, Z., Jia, C., Huang, Y., Wen, M., Liu, W., Xie, X., Liu, T., Wang, P., Shan, C., Wang, P., 2019. Mechanism analysis of organic matter enrichment in different sedimentary backgrounds: a case study of the Lower Cambrian and the Upper Ordovician-Lower Silurian, in Yangtze region. Mar. Petrol. Geol. 99, 488–497.
93. Zhang, K., Liu, R., Liu, Z.J., Li, L., Wu, X.P., Zhao, K.A., 2020a. Influence of palaeoclimate and hydrothermal activity on organic matter accumulation in lacustrine black shales from the lower cretaceous Bayingebi Formation of the Yin'e Basin, China. Palaeogeogr. Palaeoclimatol. Palaeoecol. 560 https://doi.org/10.1016/j.palaeo.2020.110007.
94. Zonneveld, K.A.F., Versteegh, G.J.M., Kasten, S., Eglinton, T.I., Emeis, K.-C., Huguet, C., Koch, B.P., de Lange, G.J., de Leeuw, J.W., Middelburg, J.J., Mollenhauer, G., Prahl, F.G., Rethemeyer, J., Wakeham, S.G., 2010. Selective preservation of organic matter in marine environments; processes and impact on the sedimentary record. Biogeosciences 7, 483–511.
95. Zou, C., Zhu, R., Chen, Z.Q., Ogg, J.G., Wu, S., Dong, D., Qiu, Z., Wang, Y., Wang, L., Lin, S., Cui, J., Su, L., Su, L., Yang, Z., 2019. Organic-matter-rich shales of China. Earth Sci. Rev. 189, 51–78.